



HAL
open science

p53-PGC-1 α Pathway Mediates Oxidative Mitochondrial Damage and Cardiomyocyte Necrosis Induced by Monoamine Oxidase-A Upregulation: Role in Chronic Left Ventricular Dysfunction in Mice

Christelle Villeneuve, Céline Guilbeau-Frugier, Pierre Sicard, Olivier Lairez, Catherine Ordener, Thibaut Duparc, Damien de Paulis, Bettina Couderc, Odile Spreux-Varoquaux, Florence Tortosa, et al.

► To cite this version:

Christelle Villeneuve, Céline Guilbeau-Frugier, Pierre Sicard, Olivier Lairez, Catherine Ordener, et al.. p53-PGC-1 α Pathway Mediates Oxidative Mitochondrial Damage and Cardiomyocyte Necrosis Induced by Monoamine Oxidase-A Upregulation: Role in Chronic Left Ventricular Dysfunction in Mice. *Antioxidants and Redox Signaling*, 2013, 18 (1), pp.5-18. 10.1089/ars.2011.4373 . inserm-02446148

HAL Id: inserm-02446148

<https://inserm.hal.science/inserm-02446148>

Submitted on 20 Jan 2020

HAL is a multi-disciplinary open access archive for the deposit and dissemination of scientific research documents, whether they are published or not. The documents may come from teaching and research institutions in France or abroad, or from public or private research centers.

L'archive ouverte pluridisciplinaire **HAL**, est destinée au dépôt et à la diffusion de documents scientifiques de niveau recherche, publiés ou non, émanant des établissements d'enseignement et de recherche français ou étrangers, des laboratoires publics ou privés.

Antioxidants & Redox Signaling

Antioxidants & Redox Signaling: <http://mc.manuscriptcentral.com/liebert/ARS>

p53-PGC-1 α pathway mediates oxidative mitochondrial damage and cardiomyocyte necrosis induced by monoamine oxidase-A upregulation: role in chronic left ventricular dysfunction in mice.

Journal:	<i>Antioxidants & Redox Signaling</i>
Manuscript ID:	Draft
Manuscript Type:	Original Research Communication
Date Submitted by the Author:	n/a
Complete List of Authors:	Villeneuve, Christelle; I2MC, cardiac remodelling Guilbeau-Frugier, Céline; I2MC, cardiac remodelling Lairez, Olivier; I2MC, cardiac remodelling Ordener, Catherine; I2MC, cardiac remodelling Duparc, Thibaut; INSERM U858, I2MR De Paulis, Damien; INSERM U886 Couderc, Bettina; Institut Claudius Regaud Spreux-Varoquaux, Odile; Université Versailles Tortosa, Florence; I2MC, cardiac remodelling Garnier, Anne; INSERM U769 Knauf, Claude; INSERM U858, I2MR Valet, Philippe; INSERM U858, I2MR Langin, Dominique; INSERM U858, I2MR Borch, Elisabetta; University of Florence, Department of Biochemical Sciences Nediani, Chiara; University of Florence, Department of Biochemical Sciences gharib, abdallah; INSERM U886 Ovize, Michel; INSERM U886; Hospices Civils de Lyon, CIC Delisle, Marie-Bernadette; I2MC, cardiac remodelling Parini, Angelo; INSERM U858 Mialet-Perez, Jeanne; INSERM, I2MC
Keyword:	Cardiovascular, Cell Survival and Death, Free Radicals, Mitochondria

SCHOLARONE™
Manuscripts

Villeneuve

Original research communication

p53-PGC-1 α pathway mediates oxidative mitochondrial damage and cardiomyocyte necrosis induced by monoamine oxidase-A upregulation: role in chronic left ventricular dysfunction in mice.

*Christelle Villeneuve,^{1,2} *Céline Guilbeau-Frugier,^{1,2} Olivier Lairez,^{1,2} Catherine Ordener,^{1,2} Thibaut Duparc,^{1,2} Damien De Paulis,^{3,4} Bettina Couderc,² Odile Spreux-Varoquaux,⁵ Florence Tortosa,^{1,2} Anne Garnier,⁶ Claude Knauf,^{1,2} Philippe Valet,^{1,2} Dominique Langin,^{1,2} Elisabetta Borchini,⁷ Chiara Nediani,⁷ Abdallah Gharib,^{3,4} Michel Ovize,^{3,4} Marie-Bernadette Delisle,^{1,2} Angelo Parini,^{1,2} and Jeanne Mialet-Perez^{1,2}

¹ INSERM ; UMR 1048 ; Institut des Maladies Métaboliques et Cardiovasculaires ; Toulouse, France

² Université Paul Sabatier ; CHU de Toulouse ; Institut Claudius Regaud, F-31432 Toulouse, France

³ INSERM ; U886 ; Université Claude Bernard Lyon 1, F-69373 Lyon, France

⁴ Service de Cardiologie, Hôpital Louis Pradel, Hospices Civils de Lyon, F-69677 Bron, France

⁵ Université Versailles-St-Quentin, Centre Hospitalier de Versailles, F-78157 Le Chesnay, France

⁶ INSERM; U-769; Université Paris-Sud, Chatenay-Malabry, France

⁷ Department of Biochemical Sciences, University of Florence, Italy

Running head: MAO-A and cardiac oxidative damage

* C. Villeneuve and C. Guilbeau-Frugier contributed equally to this work.

5607 words, 38 references, 4 color illustrations, 3 greyscale illustrations

Correspondance: Angelo Parini, INSERM UMR 1048, Institut des Maladies Métaboliques et Cardiovasculaires, BP 84225, 31432 Toulouse Cedex 4, France

Tel: 33561325601, Fax: 33561325622, e-mail: angelo.parini@inserm.fr

Villeneuve

Abstract

Aims—Oxidative stress and mitochondrial dysfunction participate together in the development of heart failure. mRNA levels of monoamine oxidase-A (MAO-A), a mitochondrial enzyme that produces H₂O₂, increase in several models of cardiomyopathies. Therefore, we hypothesized that an increase in cardiac MAO-A could generate cardiac oxidative stress and mitochondrial damage, leading to heart dysfunction.

In the present study, we evaluated the consequences of cardiac MAO-A augmentation on chronic oxidative damage, cardiomyocyte survival and heart function, and identified the intracellular pathways involved.

Results—We generated transgenic mice (Tg) with cardiomyocyte-driven MAO-A overexpression. Transgenic mice displayed cardiac MAO-A levels similar to those found in heart failure and aging. As expected, Tg mice showed a significant decrease in the cardiac amounts of the MAO-A substrates serotonin and noradrenaline. This was concomitant with enhanced H₂O₂ generation *in situ* and mitochondrial DNA oxidation. As a consequence, MAO-A Tg mice demonstrated progressive loss of cardiomyocytes by necrosis and ventricular failure, which were prevented by chronic treatment with the MAO-A inhibitor clorgyline and the anti-oxidant N-acetyl-cystein. Interestingly, Tg hearts exhibited p53 accumulation and down-regulation of PGC-1 α , a master regulator of mitochondrial function. This was concomitant with cardiac mitochondrial ultrastructural defects and ATP depletion. *In vitro*, MAO-A adenovirus transduction of neonatal cardiomyocytes mimicked the results in MAO-A Tg mice, triggering oxidative stress-dependent p53 activation, PGC-1 α down-regulation, mitochondrial impairment and cardiomyocyte necrosis.

Innovation and conclusion—We provide the first evidence that MAO-A upregulation in the heart causes oxidative mitochondrial damage, PGC-1 α /p53-dependent cardiomyocyte necrosis and chronic ventricular dysfunction.

Villeneuve

Introduction

Heart failure (HF) is among the most prevalent diseases in developed countries. Reactive oxygen species (ROS) are believed to play a prominent role in triggering ventricular damage, thus accelerating the progression of HF (10). At the molecular level, chronic exposition to ROS leads to accumulation of oxidized DNA, proteins and lipids. This results in cardiomyocyte dysfunction and death, a determining factor in ventricular remodelling and failure(8). Cardiac mitochondria are at particular risk for oxidative stress(34). To provide its high energy demand, the heart contains numerous mitochondria and is especially vulnerable to mitochondrial dysfunction. Mitochondrial oxidative damage such as DNA mutations have been related to mitochondrial dysfunction, decline in cardiomyocyte function and death(4,16,34,38). In addition, a decrease in energy metabolism in several animal models of HF and in humans has been linked to the down-regulation of PGC-1 α (28,29), a master regulator of mitochondrial function which could represent a preferential target for ROS.

Despite accumulative evidences of the deleterious effect of ROS in the failing heart, the precise sources of ROS overproduction remain to be identified. Specific targeting of ROS sources could provide a more effective therapy for HF than global anti-oxidant therapies, which have given conflicting results in clinical trials(10). Monoamine oxidase-A (MAO-A) located in the outer mitochondrial membrane of cardiomyocytes serves as a major pathway for serotonin and catecholamines metabolism and has been proposed as a relevant source of H₂O₂ in the heart. A deleterious role for MAO-A/ROS pathway has already been demonstrated in acute situations such as ischemia-reperfusion where pharmacological or genetic inactivation of MAO-A prevented cardiomyocyte death(6,26). In addition, in mice with ventricular pressure overload, genetic and pharmacological MAO-A inhibition prevented transition from hypertrophy to failure(13).

Interestingly, MAO-A mRNA expression appears to be enhanced in several models of HF(13,15) as well as in the aging rat heart(21). However, the effect and downstream targets of such chronic increase in MAO-A expression are presently unknown. To address this question, we combined *in vivo* and *in vitro*

Villeneuve

1
2
3 approaches to analyze the functional consequences of cardiomyocyte MAO-A overexpression using
4 transgenic mice (Tg) and adenoviral transduced cardiomyocytes.
5
6

7 We found that increasing MAO-A expression to pathophysiological levels observed in failing and aging
8 hearts was sufficient *per se* to cause chronic oxidative stress, mitochondrial damage and PGC-1 α down-
9 regulation, thereby contributing to cardiomyocyte necrosis. Consequently, MAO-A transgenic mice died
10 prematurely from dilated HF. Interestingly, we identified for the first time p53 and as a major signalling
11 intermediate in H₂O₂-induced mitochondrial damage, PGC-1 α downregulation and cardiomyocyte
12 necrosis linked to MAO-A activation.
13
14
15
16
17
18
19
20
21
22
23
24
25
26
27
28
29
30
31
32
33
34
35
36
37
38
39
40
41
42
43
44
45
46
47
48
49
50
51
52
53
54
55
56
57
58
59
60

Villeneuve

Results

Myocardial MAO-A activity increases during ventricular hypertrophy, failure and aging.

We first analyzed changes in myocardial MAO-A activity in response to various stresses. In a rat model of pressure overload induced by ascendant aortic banding(7), MAO-A activity was significantly increased at the stage of compensated hypertrophy (5 weeks) and decompensated HF (15 weeks), compared to age-matched sham rats (Fig. 1A). Next, we examined the effect of aging on cardiomyocyte MAO-A activity. MAO-A activity increased gradually between 2 and 24 months in cardiac homogenates (Fig. 1B). Interestingly, a strong increase in MAO-A activity was also observed in cardiac myocytes isolated from senescent rats (24-months old) compared to those isolated from 2-months old rats (Fig. 1C).

Tg mice overexpress an active MAO-A enzyme in cardiac mitochondria.

In order to mimic changes observed during ventricular pressure overload and aging, we generated mice with cardiomyocyte-specific overexpression of MAO-A under the control of the α -MHC promoter. Two independent lines of Tg mice were propagated with different levels of MAO-A activity of 9336 ± 2139 pmol/mg/min for Tg 61 and 40291 ± 11912 pmol/mg/min for Tg 113 (Fig. 2A). The levels of MAO-A expression in Tg61 were similar to those observed in failing and aging hearts (Fig. 1A, B). Western blot analysis demonstrated specific upregulation of MAO-A in cardiac but not liver homogenates compared to non transgenic littermates (NTg) (Fig. 2B). In addition, we verified that overexpressed MAO-A was correctly targeted to mitochondria and maintained its catalytic activity. Double immunofluorescence staining on heart sections showed enhanced levels of MAO-A in Tg 61 mice compared to NTg, and colocalization with the mitochondrial protein Cox IV (Fig. 2C). We also found that mitochondria isolated from Tg 61 mice produced greater amounts of H_2O_2 in presence of the MAO substrate tyramine compared to NTg, an effect that was inhibited by 96% with the MAO inhibitor pargyline (Fig. 2D). Finally, we measured by HPLC the levels of MAO-A substrates serotonin (5-HT) and norepinephrine (NE), along with their respective MAO metabolites 5-hydroxyindoleacetic acid (5-HIAA) and dihydroxyphenylglycol (DHPG) in cardiac homogenates. As shown in Fig. 2E, 2F, the ratios of 5-HIAA/5-HT and DHPG/NE

Villeneuve

1
2
3 were significantly elevated in Tg 61 mice, as a result of both substrate depletion and metabolite
4 accumulation. Altogether, our observations demonstrate that oxidative metabolism of 5-HT and NE at the
5 mitochondria is potentiated in MAO-A Tg mice.
6
7
8

9
10
11
12 *MAO-A Tg mice develop dilated cardiomyopathy.*

13
14 To evaluate the consequences of MAO-A upregulation on cardiac morphology and function,
15 echocardiographies were performed in Tg 61 mice at different ages. At 1.5 months, ventricular function
16 was not modified in Tg 61 compared to NTg mice (data not shown). However, there was a significant and
17 progressive decrease in fractional shortening (FS) in Tg 61 mice between 3 and 7 months, accompanied
18 by left-ventricular dilatation (Table 1). HF was confirmed in 7-months old Tg mice by a significant
19 increase in lung weight/body weight ratio (7.66 ± 0.47 mg/g vs 5.41 ± 0.27 mg/g, $p < 0.05$) compared to NTg,
20 indicative of pulmonary congestion. As a consequence, life-span was severely reduced in Tg 61 mice with
21 a maximum survival around 9 months (suppl Fig. 1). To demonstrate that the deleterious effects of MAO-
22 A upregulation depended on its catalytic activity, we performed echocardiographies on Tg mice treated
23 with the MAO-A inhibitor clorgyline from the age of 1 to 5 months. Chronic administration of clorgyline
24 (10 mg/kg/day) prevented LV dysfunction and chamber dilatation in Tg mice, compared to untreated Tg
25 mice (Table 1). It is noteworthy that another line of Tg mice (Tg 113), which express a higher amount of
26 MAO-A, shows an accelerated cardiomyopathy, with a dramatic drop in FS at 2 months, ventricular
27 dilatation and decreased survival (Suppl Fig. 1, 2A). Altogether, our data demonstrate that an increase in
28 MAO-A catalytic activity induces progressive dilated cardiomyopathy and HF in mice.
29
30
31
32
33
34
35
36
37
38
39
40
41
42
43
44
45
46
47
48

49 *Evidences of cell death in the hearts of MAO-A Tg mice, accompanied by inflammatory response, reactive*
50 *cellular hypertrophy and fibrosis.*

51
52 To gain more insights into the deleterious effects of myocardial MAO-A upregulation, we performed
53 histological examinations. The most striking features in Tg hearts were myocardial disarray (Fig. 3A,
54 upper panel) and cardiomyocytes drop-out, which started around the age of 1.5 months (-16 %, non-
55
56
57
58
59
60

Villeneuve

1
2
3 significant) and reached -48 % ($p < 0.01$) at the age of 3 months, compared to NTg mice. As a
4
5 compensatory response, residual cardiomyocytes were hypertrophied and interstitial fibrosis was
6
7 enhanced in Tg mice (Fig. 3A, 3B). Chronic MAO-A inhibition with clorgyline prevented cardiomyocyte
8
9 drop-out, hypertrophy and fibrosis in Tg mice (Fig. 3A, 3B). Interestingly, histological findings were
10
11 recapitulated in Tg 113 mice (Suppl Fig. 2). In addition, Tg 61 cardiac mRNA expression analysis
12
13 confirmed histological findings, with up-regulation of pro-inflammatory cytokines as soon as 1.5 months
14
15 after birth, re-expression of the fetal gene program and upregulation of extracellular matrix components
16
17 (Suppl Fig. 3).
18
19

20
21 To clarify the underlying mechanism of myocyte death between 1.5 and 3 months in Tg mice, we tested
22
23 for the presence of apoptosis and necrosis. Histological observations highlighted necrotic areas with
24
25 disruption of myofibrils, cell debris, loss of nuclei, smudging and scattered leukocytes (see arrow in Fig.
26
27 3A). Accordingly, plasmatic levels of troponin-I (a sensitive marker of myocyte necrosis) were greatly
28
29 increased in young Tg mice, while they were undetectable in NTg mice (Fig. 3C). Concerning apoptosis,
30
31 TUNEL staining or caspase-3 cleavage were not modified in 1.5 months-old Tg mice, albeit a small
32
33 increase in the number of apoptotic nuclei was observed at 3 months (Fig. 3D, 3E). In contrast, the
34
35 expression of the cell death intermediate p53 was significantly increased in Tg hearts compared to NTg
36
37 (Fig. 3F). As p53 is known to participate, not only in apoptotic but also in necrotic death
38
39 induction(35,37), our results suggest that it could be linked to cardiomyocyte necrosis in MAO-A Tg
40
41 mice. Altogether, our results point toward cell necrosis as the predominant mechanism for cardiomyocyte
42
43 drop-out in MAO-A overexpressing mice.
44
45
46
47
48

49 *Real-time H₂O₂ generation and oxidative stress are increased in hearts from MAO-A Tg mice and*
50
51 *participate in the development of dilated cardiomyopathy.*
52

53 In order to determine whether H₂O₂ was overproduced in Tg 61 mice, we used an H₂O₂-sensitive
54
55 electrode which detects real-time generation of H₂O₂ *in situ* by an amperometric method. As shown in
56
57 Fig. 4A, *in vivo* levels of H₂O₂ were significantly increased in ventricles from anesthetized 1.5 months-
58
59
60

Villeneuve

old Tg mice compared to NTg mice. Next, we evaluated DNA oxidation, a sensitive marker of oxidative stress, in cardiac sections from Tg 61 mice using 8-OH-dG staining. We found that DNA oxidation was significantly increased in Tg hearts compared to NTg hearts (Fig. 4B). Interestingly, a prominent cytoplasmic staining indicated that mitochondrial DNA was particularly susceptible to oxidation in this model. Chronic treatment of Tg mice with clorgyline prevented accumulation of 8-OH-dG (Fig. 4B). Then, we analyzed the regulation of anti-oxidant defenses in cardiac homogenates from NTg and Tg mice. Interestingly, we found that the activity of two enzymes specifically involved in H₂O₂ degradation, glutathion peroxidase (GPX) and catalase (CAT), were modified in Tg mice while superoxide dismutase (Mn-SOD) activity remained unchanged (Fig. 4C). To evaluate the participation of oxidative stress in the onset of cardiac dysfunction associated with MAO-A upregulation, we used a pharmacological approach with N-acetyl-cystein (NAC), a ROS scavenger. Chronic treatment with 1.5 g/kg/day of NAC from 1 to 6 months preserved cardiac function (FS) in Tg mice at a level comparable to NTg mice, and prevented cardiac dilatation (LVESD) (Fig. 4D). Most interestingly, cell loss was also prevented (Fig. 4D). Altogether, our results provide evidence that chronic H₂O₂ generation by MAO-A induces progressive oxidative damage, cardiomyocyte drop-out and deterioration of cardiac function in Tg mice.

Upregulation of MAO-A is associated with mitochondrial damage in the heart.

Mitochondrial dysfunction plays a major role in HF. Since MAO-A is located in the outer membrane of mitochondria, and mitochondrial DNA is oxidized in Tg mice, we hypothesized that this organelle could be at particular risk for H₂O₂-mediated injury. Expression profiling using microarrays indicated a global down-regulation of genes encoding mitochondrial proteins, and emphasized depressed energy metabolism and oxidative phosphorylation in Tg mice accompanied by the downregulation of the PGC-1 α pathway (Fig. 5A, for a list of genes see Suppl. Table 2, 3). Therefore, we examined mitochondrial ultrastructure by electronic microscopy in Tg mice at the age of 1.5 months. In NTg mice, mitochondria were normal with dense matrices filled, homogeneous matrix granules, intact double membrane and tightly packed cristae (Fig. 5B, left panel). In contrast, Tg heart mitochondria tended to make aggregates and were

Villeneuve

heterogeneous in size (Fig. 5B, right panel). In the same cell, small and numerous mitochondria were observed, alternating with normal or swelling mitochondria. The most obvious change was the appearance of electron-lucent areas in mitochondrial matrix and concentric cristae. These morphological features indicated mitochondrial damage. Accordingly, ATP content was decreased in myocardial samples from 1.5 months-old Tg mice, suggesting early impairment in mitochondrial bioenergetics (Fig. 5C). Finally, using real-time RT-PCR, we confirmed that expression of PGC-1 α , a master regulator of mitochondrial biogenesis, was significantly downregulated in Tg mice at 1.5 months (Fig. 5D).

Upregulation of MAO-A sensitizes cardiomyocytes to necrosis through p53 activation.

To gain insight into the mechanism involved in MAO-A-dependent cell necrosis, we developed an *in vitro* model of MAO-A adenoviral vector (AdeMAO-A) transduction in neonatal cardiomyocytes. AdeMAO-A transduction (MOI 5) induced a significant increase in MAO-A activity in cardiomyocytes (Fig. 6A). Interestingly, application of NE (24 hours) induced cardiomyocyte necrosis only in cells transduced with AdeMAO-A, as demonstrated by LDH release (Fig. 6B). Thus, as observed in Tg mice, in the presence of a constant substrate concentration, an increase in MAO-A activity sensitized cardiomyocytes to necrosis. We confirmed this finding with tyramine, another MAO substrate devoided of membrane receptors in the mammalian heart. Tyramine application for 24 hours promoted necrosis and oxidative stress in cardiomyocytes transduced with AdeMAO-A (MOI 5), which were both prevented by clorgyline and NAC (Fig. 6C, Suppl Fig.4). As we observed a significant accumulation of p53 in Tg hearts compared to NTg (Fig 3F), we hypothesized that this protein could play an important role in MAO-A-dependent cell necrosis. We examined the kinetic of p53 activation in AdeMAO-A-transduced cardiomyocytes in the presence of tyramine. Interestingly, tyramine treatment induced a rapid increase in phospho(ser15)-p53 (Fig. 6D), which was dependent on ROS generation since it was reversed in the presence of NAC (Fig. 6E). Expression of total p53 was also significantly increased following 6 hours of tyramine treatment (Fig. 6D). Therefore, we tested whether p53 activation played a role in MAO-A-dependent necrosis by a siRNA approach. As shown in Fig. 6F, p53 siRNA transfection inhibited p53

Villeneuve

1
2
3 protein expression at 48 and 72 hours compared to Scr-transfected cells. As a consequence, induction of
4 necrosis was significantly reduced in p53-silenced cardiomyocytes compared to Scr (Fig. 6F). Tyramine-
5 induced LDH release was also significantly reduced in cardiomyocytes treated with a pharmacological
6 p53 inhibitor, pifithrin- α , compared to vehicle-treated cardiomyocytes (Fig. 6G). In conclusion, our data
7 demonstrate for the first time that p53 activation plays a major role in MAO-A-mediated cardiomyocyte
8 necrosis.
9
10
11
12
13
14
15
16
17
18

19 *Mitochondrial damage and PGC-1 α downregulation are key events in MAO-A-dependent cardiomyocyte*
20 *necrosis, which are both dependent on p53 activation.*
21
22

23 Early mitochondrial impairment was found in MAO-A in Tg mice. Thus, we asked whether MAO-A
24 activation could be responsible for mitochondrial damage *in vitro*. As shown in Fig. 7A, as soon as 4
25 hours following tyramine application, mitochondrial ultrastructure was severely impaired in AdeMAO-A-
26 transduced cardiomyocytes. These ultrastructural alterations fitted with ATP depletion and PGC-
27 1 α down-regulation, indicating a rapid decline in cell metabolic function (Fig. 7B,C). Therefore, we
28 asked whether p53 contributed to MAO-A-induced mitochondrial damage. Most interestingly, p53
29 silencing attenuated mitochondrial ultrastructural defects (Fig 7A) and PGC-1 α down-regulation (Fig.
30 7C) compared to Scr-transfected cells. This is consistent with recent data that identified p53 as an
31 important and direct repressor of PGC-1 α in the heart, an event that participates in the functional decline
32 of cardiac function during aging(30). We thus evaluated the importance of PGC-1 α down-regulation in
33 MAO-A mediated cell necrosis by restoring PGC-1 α levels in cardiomyocytes. Co-transduction of PGC-
34 1 α adenoviral vector (AdePGC-1 α) with AdeMAO-A almost completely prevented tyramine-induced
35 LDH release in cardiomyocytes (Fig. 7D). Thus, our results demonstrate that an increase in MAO-A
36 activity sensitizes cardiomyocytes to mitochondrial damage, metabolic decline and cell necrosis. In
37 addition, p53-dependent repression of PGC-1 α in cardiomyocytes constitutes an important step in MAO-
38 A-dependent necrosis (Fig. 7E).
39
40
41
42
43
44
45
46
47
48
49
50
51
52
53
54
55
56
57
58
59
60

Villeneuve

Discussion

In the present study, we demonstrate for the first time that a chronic increase in MAO-A engenders mitochondrial oxidative damage, PGC-1 α down-regulation, myocyte necrosis and HF. Importantly, we report that p53 acts as a major downstream effector of MAO-A-dependent mitochondrial injury, PGC-1 α downregulation, and myocyte necrosis.

Our observation that enhanced MAO-A activity *per se* is sufficient to trigger deleterious effects in the heart represents a new finding, particularly relevant in cardiac diseases where MAO-A upregulation appears to be frequently observed(13,15). We found that MAO-A activity was increased in rat heart during pressure overload induced hypertrophy and failure, and during cardiac aging. Indeed, the level of MAO-A activity in failing hearts was about 6500 pmol/mg/min, which is in the same order of magnitude than in Tg mice (line 61, 9336 pmol/mg/min). At present, the rationale for MAO-A upregulation during cardiac stress remains unknown. Sympathetic activation and NE spillover are major features associated with cardiac aging and failure(9,14). In addition, whole-blood 5-HT levels increase in failing humans hearts(25). Therefore, MAO-A upregulation might be an adaptative mechanism to increased levels of substrates, as previously demonstrated in rat mesangial cells(27). However, on the long term, a chronic increase in 5-HT and catecholamines metabolism by cardiac MAO-A could induce oxidative stress and cardiomyocyte toxicity. Understanding the mechanisms of MAO-A upregulation in the heart seems of major interest and will need to be elucidated in future studies.

Here, we provided evidence that oxidative stress played a key role in cardiomyocyte drop-out and HF in Tg mice. First, using an original approach of direct real-time H₂O₂ detection in mice heart, we showed that Tg mice were constantly exposed to high H₂O₂ cardiac level. This observation correlated with the appearance of DNA oxidative damage in Tg hearts. Second, chronic treatment with an anti-oxidant (NAC) prevented cardiomyocyte death and cardiac failure. Altogether, our results put forward that MAO-A upregulation represents an endogenous system of chronic ROS generation leading to heart dysfunction.

Villeneuve

This is in accordance with a recent study demonstrating a protective effect of MAO-A inhibition on cardiac oxidative stress and failure during pressure overload(13).

When examining MAO-A induced cardiomyocyte death, apoptotic nuclei were barely detectable in young Tg mice. Considering that caspase-3 was not activated in Tg hearts, we concluded that such level of apoptosis was insufficient to explain the major cardiomyocyte loss observed in Tg mice. On the other hand, we found that necrosis was strongly enhanced in Tg hearts, as assessed by histological examinations and plasma troponin-I measurement. Moreover, MAO-A overexpression *in vitro* rendered the cardiomyocytes more vulnerable to necrosis in the presence of NE and tyramine. According to its concentration, H₂O₂ has been demonstrated to induce either apoptosis or necrosis in cardiomyocytes(17).

In addition, human aged cells with accumulative oxidative damages are more sensitive to necrosis(23). Therefore, MAO-A up-regulation during cardiac failure or aging could sensitize cardiomyocytes to necrosis. This observation is interesting since, after being neglected for a while, necrosis is now recognized as a major way of cell death during chronic HF(24). Hence, elucidating necrotic signalling cascades in the heart seems of major interest. Here, we provide evidence that p53 accumulates in the hearts of Tg mice and can be rapidly activated by tyramine *in vitro*. Both pharmacological and siRNA approaches demonstrated its involvement in cardiomyocyte necrosis induced by MAO-A. The identification of p53 as a mediator of cardiomyocyte necrosis in response to oxidative stress is consistent with accumulating evidences demonstrating an important role of p53 in HF(20,31,33). In addition, apart from being a well known pro-apoptotic factor, p53 has been demonstrated to participate in cell necrosis induced by DNA damage or TNF α (35,37).

Based on our observations, overexpression of MAO-A *in vitro* and *in vivo* was associated with mitochondrial ultrastructural defects, ATP depletion and PGC-1 α downregulation. *In vitro*, p53 silencing prevented tyramine-induced mitochondrial damage and PGC-1 α downregulation, indicating that p53 activation played a key role in amplifying mitochondrial injury in response to MAO-A/H₂O₂.

Interestingly, such link between mitochondrial oxidative damage and p53 activation has been recently

Villeneuve

1
2
3 observed in a model of HF induced by doxorubicin(36). Down-regulation of PGC-1 α in our model is
4
5 interesting since it has been reported to contribute to the maladaptive energetic profile of failing
6
7 hearts(28). Notably, we found that restoring PGC-1 α expression with adenoviral transduction protected
8
9 cardiomyocytes from MAO-A-induced necrosis. This beneficial effect of PGC-1 α upregulation could be
10
11 attributed to enhanced mitochondrial biogenesis/bioenergetics(3) or upregulation of antioxidant enzymes,
12
13 as previously described(19).
14
15

16
17 In conclusion, our results demonstrate that enhancing MAO-A expression, as observed in different
18
19 models of cardiomyopathy, induces the activation of p53, which acts as a repressor of PGC-1 α expression
20
21 and contributes to bioenergetic defects and mitochondrial damage leading to cardiomyocyte necrosis (Fig.
22
23 7E). These findings put forward that an increase in cardiac MAO-A could play a major role in the
24
25 progression of HF, and propose MAO-A as a promising target for the prevention of cardiomyocyte death
26
27 in chronic diseases.
28
29
30
31
32
33
34
35
36
37
38
39
40
41
42
43
44
45
46
47
48
49
50
51
52
53
54
55
56
57
58
59
60

Villeneuve

Innovation

Oxidative stress and mitochondrial dysfunction participate together in the development of HF but the precise source and mechanisms of action are still a matter of debate. In the present manuscript, we show for the first time that enhancing MAO-A expression, as observed in different models of cardiomyopathy, causes oxidative mitochondrial damage, PGC-1 α /p53-dependent cardiomyocyte necrosis and chronic ventricular dysfunction leading to HF.

Villeneuve

Materials and methods

Generation of Tg mice. The cDNA encoding rat MAO-A (genbank NM_033653) provided by Akio Ito (Kyushu University, Japan) was subcloned into the full-length mouse α -myosin heavy-chain (α -MHC) promoter. Briefly, a 2060 bp cDNA, including 6 bp of the 5' and 474 bp of the 3' flanking sequences was subcloned into the Sall site of the polylinker of the α -MHC promoter construct(12). The resulting recombinant plasmid p α MHC-MAO-A, was confirmed by restriction mapping and nucleotide sequencing. A linear 8000 bp DNA fragment was microinjected into fertilized eggs at the "Institut Clinique de la Souris" (Strasbourg, France). Offsprings were genotyped and founders were bred with C57BL6/J mice to establish stable Tg mice. Mice were housed in a pathogen-free facility and handled in accordance with the principles and procedures outlined in Council Directive 86/609/EEC. For all experiments, littermates were used as controls.

Assays of MAO activity. MAO-A activities in cardiac tissues were performed as previously described(18). For *in vitro* assays, 5 μ g of cellular lysates were incubated with 20 μ mol/L MAO-A substrate (MAO-Glo Assay kit, Promega, France) for 20 min at 37°C and non-specific activity was defined in the presence of clorgyline.

Primary cultures of cardiomyocytes. Adult ventricular myocytes were obtained from hearts of male Sprague-Dawley rats at the ages of 2, 12 and 24 months with retrograde perfusion, as previously described(6). For neonatal cardiomyocytes, hearts of 2-3 days old Sprague-Dawley rats were dissociated with collagenase type II, 0.1 % (Biovalley), as previously described(26). Myocyte enrichment was performed by centrifugation through a discontinuous Percoll gradient and resultant suspension of myocytes was plated onto gelatin-coated culture dishes. 24 h following adenovirus transduction, medium was replaced with Ham-F12 medium supplemented with dialysed-FCS 3% and inhibitors (clorgyline, NAC, pifithrin- α), when indicated. Tyramine was added 2 h later for the indicated time. The selected siRNA for p53 is an ON-TARGET plus SMART pool siRNA (Dharmacon, Surrey, United Kingdom).

Villeneuve

SiRNAs were transfected 24 hours before AdeMAO-A adenovirus transduction, using the Dharmafect reagent according to the manufacturer's recommendations.

Western blot. Ventricular homogenates and cardiomyocyte extracts were electrophoresed and transferred as described(18). Membranes were incubated with anti-MAO-A, anti-GAPDH antibodies (Santa Cruz Biotechnology, Heidelberg, Germany) or anti-caspase-3, anti-p53, anti-phospho-p53 antibodies (Cell Signaling, Danvers, USA).

Immunofluorescence. Frozen cardiac sections were fixed with PFA 3% for 15 min and neutralized with glycine 100 mmol/L. Following permeabilization with Triton 0.5 %, heart sections were incubated first with MAO-A antibody overnight at 4°C, and CoxIV antibody (Santa Cruz Biotechnology, Heidelberg, Germany) at room temperature (RT) for 1 h. After washing, sections were incubated for 1 h at RT with Oregon Green 488-conjugated goat anti-rabbit or Alexa 594-conjugated goat anti-mouse antibodies (Invitrogen, Cergy Pontoise, France). Image acquisition was performed using a DM600 microscope (Leica) fitted with a Roper COOLsnap ES CCD camera. Images were denoised using the Nearest Neighbours approach of the 2D Deconvolution setup of Metamorph software (Filter size: 2; Scaling Factor: 0.5; Result Scale : 2).

Heart H₂O₂ real-time measurement. The H₂O₂-specific amperometric probe was calibrated as referred to manufacturer's instructions (ISO-HPO-100; World Precision Instruments, Aston, UK). Briefly, the probe was left in 20 ml of PBS buffer. After the sensor had stabilized, solution of H₂O₂ (from 100 to 800 nM) was added in the PBS solution. The current observed was directly proportional to H₂O₂ concentration. The sensitivity of a fresh probe was at least 1 pA/nM. Probes were tested before each experiment to validate their sensitivity. Then, 1.5 months-old mice were given pentobarbital (100 mg/kg ip) and were placed on a heating plate at 37°C. The chest was opened quickly and the probe was implanted in the left ventricle to monitor H₂O₂ release. After 20 min of stabilization of the probe, H₂O₂ concentration in the tissue was measured for 15 min in real-time with the data acquisition system LabTrax (WPI) connected to the free radical analyzer Apollo1000 (WPI). Data acquisition and analysis were performed with DataTrax2 software (WPI).

Villeneuve

Electron microscopy. Left ventricles of mice were cut in cubes of 1 mm³ and placed in glutaraldehyde 2.5%. Semi-thin (1 μm) sections were stained with toluidine blue. Trimmed ultra-thin sections (600 Å) were stained with uranyl acetate and lead citrate. Sections were examined under a transmission electron microscopy (Hitachi 5HU12A).

Mitochondrial H₂O₂ production. Cardiac mitochondria were isolated using the procedure of Gomez et al.(11). Total H₂O₂ production was measured using a fluorimeter F-2500 (Hitachi) and a fluorescent probe Amplex Red[®] (10 μmol/L) in the presence of 0.6 U/ml horseradish peroxidase (excitation and emission wavelengths set to 530 and 590 nm, respectively).

Assays of 5-HT, 5-HIAA, NE and DHPG. Snap-frozen ventricular tissues were homogeneously grinded in 1.5 ml water. Assays for 5-HT, 5-HIAA(2), and NE, DHPG(5) were performed using two different HPLC methods with coulometric detection applied to tissues. For 5-HT and 5-HIAA, determinations were made without extraction on the centrifugated supernatants after deproteinization of the aqueous mixture using HClO₄ 0.1 mol/L and ascorbic acid 3.10⁻⁴ mol/L. For NE and DHPG determinations, 500 μl samples of the aqueous centrifugated mixture were extracted using acid-washed alumina columns.

Echocardiography. Animals were anesthetized with 2% isoflurane and examined with non invasive echocardiography (echocardiograph Vivid 7 ultrasound, GE). Cardiac ventricular dimensions were measured on M-mode images at least 5-times for the number of animals indicated.

Histological analysis. Ventricles were incubated in Carnoy's fixative solution (Ethanol 60%, chloroform 30%, acetic acid 10%), embedded in paraffin and transversally sectioned. 5 μm tissue sections were stained with H&E, Masson's Trichrome or PAS. Fibrosis was measured as positively stained area with Masson's Trichrome (green), and expressed as percent of total area, using a computer-based morphometric analysis (Nis-element, Nikon). Cardiomyocyte diameter was evaluated after coloration with PAS (250-300 cells counted per heart) on left ventricle. Number of cardiomyocytes per total myocardial area was measured using manual-counting function of the analysis software in 3 consecutive areas of the left ventricle. For 8-OH-dG (a marker of nuclear and mitochondrial DNA oxidation) immunohistochemistry, antigen retrieval was performed using citrate solution (sodium citrate 1 mol/L,

Villeneuve

1
2
3 citric acid 1 mol/L, pH 6.0) at 97°C during 40 min. After washing with deionised water, endogenous
4 peroxidase activity was blocked with H₂O₂ 30 % for 10 min. 8-OH-dG mouse monoclonal antibody
5 (1:200) (AbCys, Paris, France) was incubated for 2 h at 37°C and secondary antibody for 30 min at RT.
6 Slides were washed and incubated with 1:50 DAB in substrate buffer for 5 min, and then counterstained
7 with 1:4 Mayer's haematoxylin. Positively stained area was quantified using a computer-based
8 morphometric analysis (Nis-element, Nikon) and calculated as percent of total area. Apoptosis was
9 evaluated by TUNEL staining on cardiac sections as previously described(6).

10
11
12 *Real-time RT-PCR.* Extraction of RNA from cardiac ventricles was performed using column affinity
13 purification (Qiagen, Courtaboeuf, France). cDNAs were synthesized using the superscript II RT-PCR
14 system (Invitrogen) with random hexamers. Real-time PCR was performed on a StepOnePlus system
15 (Applied Biosystem, Courtaboeuf, France) in 96-well plates with specific primers and SYBR green mix
16 (Eurogentec, Angers, France). The primers were as followed: mouse PGC-1 α -F:
17 ACGGTTTACATGAACACAGCTGC, mouse PGC-1 α -R: CTTGTTCGTTCTGTTTCAGGTGC, Rat
18 PGC-1 α -F: CACCAAACCCACAGAGAACAG, Rat PGC-1 α -R: GCAGTTCCAGAGAGTTCCACA
19
20
21
22
23
24
25
26
27
28
29
30
31
32
33

34 *Plasmatic troponin.* Plasmatic troponin-I was detected using an ELISA kit according to the
35 manufacturer's instructions (Life Diagnostic, West Chester, USA). Briefly, plasma samples were
36 incubated for 1 h at RT with an HRP-conjugated anti-cTn-I antibody in microtiter wells. After extensive
37 wash, HRP substrate was added in each well for 20 min at RT and the reaction stopped with HCl 1mol/L.
38 Absorbance was measured at 450 nm and plasmatic cTn-I concentration was determined using cTn-I
39 standards.
40
41
42
43
44
45
46

47 *Antioxidant enzyme activities.* Catalase (CAT) activity was determined by the procedure of Aebi(1). For
48 Glutathion Peroxidase (GPX) and Superoxide Dismutase (Mn-SOD), activities were evaluated as
49 previously described(32).
50
51
52

53 *Microarray analysis.* Total RNA was prepared as described above. The quality of samples was verified
54 with Agilent Bioanalyzer 6000 (Agilent Technologies, Massy, France). Hybridization of RNA was done
55
56
57
58
59
60

Villeneuve

on Agilent Mouse Genome CGH 44K chip at the Genotoul Biopuces Plate-forme (Toulouse, France).

Raw data (median values) were normalized and processed using the R statistical software and the limma package for microarrays. Weights were attributed to flag bad data points and the remaining values were

Loess-normalized within arrays and quantile-normalized between arrays. Limma was used to generate

log₂ ratios (coefficients) and p-values (using eBayes) in order to select genes with differential expression

between groups that were also well behaved in terms of expression within each individual group. Using a

log₂ ratio of 0.5 (fold-change 1.4) and a p-value cutoff of 0.005, genes were selected for analysis.

GeneSet Enrichment Analysis for categorical feature overrepresentation in each gene list (upregulated or down-regulated) was performed using Toppgene (<http://toppgene.cchmc.org/>). For each enriched

Geneset, the enrichment P-value for non-random list intersection (using Bonferroni p-value correction)

was converted to a significance score [$S = -\log(pval)$] and a matrix was constructed with colors scaled to

significance scores. Common themes were defined among the various overlapping and unique Genesets.

ATP measurement. Snap-frozen cardiac samples (30 mg) were homogenized in 500 μ l ice-cold perchloric

acid (10% v/v), sited on ice for 10 min and centrifuged at 14 000 rpm for 10 min at 4°C. Supernatants

were neutralized with KOH 2.5 mol/L and centrifuged at 4500 rpm for 5 min. Supernatants from cardiac

sample extraction or cell lysates were assayed for ATP assay kit (Bioluminescence assay kit HS II,

Roche).

Adenoviral constructs. AdePGC-1 α was described previously(22). Replication-deficient (Δ E1, E3)

adenoviral vector expressing MAO-A coding region (1.9 kb) under the control of the CMV promoter was

constructed with the AdEasy System (Qbiogen, F). Replication-defective MAO-A adenovirus (AdeMAO-

A) was generated by transfection of 293A cells with a single isolate of recombinant adenoviral vector,

expanded, and purified. Viral titers were initially determined by optical absorbance at 260 nm. Infections

were done at a certain MOI based on this definition, e.g. 1×10^6 bav/ 1×10^6 cells = MOI 1.

Intracellular ROS measurement. Generation of ROS in cardiomyocytes was evaluated using DCFDA

probe as previously described(6).

Villeneuve

1
2
3 *LDH release assay.* For quantitative assessment of cardiomyocyte necrosis, Lactate Dehydrogenase
4
5 (LDH) release in culture medium was measured using LDH-cytotoxicity Assay Kit according to the
6
7 manufacturer's instructions (Biovision).
8

9
10 *Statistical Analysis.* Results are expressed as mean±SEM. Experimental groups were compared using
11
12 Student's *t* test or 1-way ANOVA, as appropriate. A value of $p < 0.05$ was considered significant.
13
14
15
16
17
18
19
20
21
22
23
24
25
26
27
28
29
30
31
32
33
34
35
36
37
38
39
40
41
42
43
44
45
46
47
48
49
50
51
52
53
54
55
56
57
58
59
60

Villeneuve

Acknowledgements

This work was supported by grants from INSERM, Agence Nationale pour la Recherche (ANR), Fondation pour la Recherche Medicale (FRM), Mouse Clinical Institute (MCI) in Strasbourg and Région Midi-Pyrénées. We thank J. S. Iacovoni for bioinformatics. We thank A. Colom (INSERM UMR1048) and E. Couture-Lepetit (INSERM U886) for technological assistance. We thank F. Lezoualc'h (INSERM UMR1048) for critical reading of the manuscript.

Author Disclosure Statement: No competing financial interests exist

Villeneuve

List of abbreviations.

Ade: adenovirus; Clorg: clorgyline, CoxIV: cytochrome c oxidase IV, DHPG: dihydroxyphenylglycol;
FS: fraction shortening; 5-HIAA: 5-hydroxyindoleacetic acid; HPLC: High Performance Liquid
Chromatography, 5-HT: 5-hydroxy-tryptamine; LDH: lactate dehydrogenase; LV: left ventricle; LVESD:
left ventricular end-systolic diameter; MAO-A: monoamine oxidase-A; MHC: myosin heavy chain; MOI:
multiplicity of infection; NAC: N-acetyl-cystein; NE: norepinephrine; Ntg: non transgenic; PGC-1 α :
Peroxisome Proliferator-Activated Receptor- γ coactivator-1 α ; PWT: posterior wall thickness; ROS:
reactive oxygen species; Tg: transgenic, TUNEL: Terminal Deoxynucleotidyl Transferase dUTP Nick
End Labeling.

Villeneuve

References

1. Aebi H. Catalase in vitro. *Methods Enzymol.* 105: 121-126, 1984.
2. Alvarez JC, Bothua D, Collignon I, Advenier C, Spreux-Varoquaux O. Simultaneous measurement of dopamine, serotonin, their metabolites and tryptophan in mouse brain homogenates by high-performance liquid chromatography with dual coulometric detection. *Biomed Chromatogr* 13: 293-8, 1999.
3. Arany Z, He H, Lin J, Hoyer K, Handschin C, Toka O, Ahmad F, Matsui T, Chin S, Wu PH, Rybkin, II, Shelton JM, Manieri M, Cinti S, Schoen FJ, Bassel-Duby R, Rosenzweig A, Ingwall JS, Spiegelman BM. Transcriptional coactivator PGC-1 alpha controls the energy state and contractile function of cardiac muscle. *Cell Metab* 1: 259-71, 2005.
4. Barja G, Herrero A. Oxidative damage to mitochondrial DNA is inversely related to maximum life span in the heart and brain of mammals. *Faseb J* 14: 312-8, 2000.
5. Berlin I, Said S, Spreux-Varoquaux O, Olivares R, Launay JM, Puech AJ. Monoamine oxidase A and B activities in heavy smokers. *Biol Psychiatry* 38: 756-61, 1995.
6. Bianchi P, Kunduzova O, Masini E, Cambon C, Bani D, Raimondi L, Seguelas MH, Nistri S, Colucci W, Leducq N, Parini A. Oxidative stress by monoamine oxidase mediates receptor-independent cardiomyocyte apoptosis by serotonin and postischemic myocardial injury. *Circulation* 112: 3297-305, 2005.
7. De Sousa E, Veksler V, Minajeva A, Kaasik A, Mateo P, Mayoux E, Hoerter J, Bigard X, Serrurier B, Ventura-Clapier R. Subcellular creatine kinase alterations. Implications in heart failure. *Circ Res* 85: 68-76, 1999.
8. Dorn GW, 2nd. Apoptotic and non-apoptotic programmed cardiomyocyte death in ventricular remodelling. *Cardiovasc Res* 81: 465-73, 2009.
9. Eisenhofer G, Friberg P, Rundqvist B, Quyyumi AA, Lambert G, Kaye DM, Kopin IJ, Goldstein DS, Esler MD. Cardiac sympathetic nerve function in congestive heart failure. *Circulation* 93: 1667-76, 1996.
10. Giordano FJ. Oxygen, oxidative stress, hypoxia, and heart failure. *J Clin Invest* 115: 500-8, 2005.
11. Gomez L, Paillard M, Thibault H, Derumeaux G, Ovize M. Inhibition of GSK3beta by postconditioning is required to prevent opening of the mitochondrial permeability transition pore during reperfusion. *Circulation* 117: 2761-8, 2008.
12. Gulick J, Subramaniam A, Neumann J, Robbins J. Isolation and characterization of the mouse cardiac myosin heavy chain genes. *J Biol Chem* 266: 9180-5, 1991.
13. Kaludercic N, Takimoto E, Nagayama T, Feng N, Lai EW, Bedja D, Chen K, Gabrielson KL, Blakely RD, Shih JC, Pacak K, Kass DA, Di Lisa F, Paolocci N. Monoamine oxidase A-mediated enhanced catabolism of norepinephrine contributes to adverse remodeling and pump failure in hearts with pressure overload. *Circ Res* 106: 193-202.
14. Kaye D, Esler M. Sympathetic neuronal regulation of the heart in aging and heart failure. *Cardiovasc Res* 66: 256-64, 2005.
15. Kong SW, Bodyak N, Yue P, Liu Z, Brown J, Izumo S, Kang PM. Genetic expression profiles during physiological and pathological cardiac hypertrophy and heart failure in rats. *Physiol Genomics* 21: 34-42, 2005.
16. Kujoth GC, Hiona A, Pugh TD, Someya S, Panzer K, Wohlgemuth SE, Hofer T, Seo AY, Sullivan R, Jobling WA, Morrow JD, Van Remmen H, Sedivy JM, Yamasoba T, Tanokura M, Weindruch R, Leeuwenburgh C, Prolla TA. Mitochondrial DNA mutations, oxidative stress, and apoptosis in mammalian aging. *Science* 309: 481-4, 2005.
17. Kwon SH, Pimentel DR, Remondino A, Sawyer DB, Colucci WS. H(2)O(2) regulates cardiac myocyte phenotype via concentration-dependent activation of distinct kinase pathways. *J Mol Cell Cardiol* 35: 615-21, 2003.
18. Lairez O, Calise D, Bianchi P, Ordener C, Spreux-Varoquaux O, Guilbeau-Frugier C, Escourrou G, Seif I, Roncalli J, Pizzinat N, Galinier M, Parini A, Mialet-Perez J. Genetic deletion of MAO-

Villeneuve

- 1
2
3 A promotes serotonin-dependent ventricular hypertrophy by pressure overload. *J Mol Cell*
4 *Cardiol* 46: 587-95, 2009.
- 5 19. Lu Z, Xu X, Hu X, Fassett J, Zhu G, Tao Y, Li J, Huang Y, Zhang P, Zhao B, Chen Y. PGC-1
6 alpha regulates expression of myocardial mitochondrial antioxidants and myocardial oxidative
7 stress after chronic systolic overload. *Antioxid Redox Signal* 13: 1011-22.
- 8 20. Matsusaka H, Ide T, Matsushima S, Ikeuchi M, Kubota T, Sunagawa K, Kinugawa S, Tsutsui H.
9 Targeted deletion of p53 prevents cardiac rupture after myocardial infarction in mice. *Cardiovasc*
10 *Res* 70: 457-65, 2006.
- 11 21. Maurel A, Hernandez C, Kunduzova O, Bompert G, Cambon C, Parini A, Frances B. Age-
12 dependent increase in hydrogen peroxide production by cardiac monoamine oxidase A in rats. *Am*
13 *J Physiol Heart Circ Physiol* 284: H1460-7, 2003.
- 14 22. Mazzucotelli A, Ribet C, Castan-Laurell I, Daviaud D, Guigne C, Langin D, Valet P. The
15 transcriptional co-activator PGC-1alpha up regulates apelin in human and mouse adipocytes.
16 *Regul Pept* 150: 33-7, 2008.
- 17 23. Miyoshi N, Oubrahim H, Chock PB, Stadtman ER. Age-dependent cell death and the role of ATP
18 in hydrogen peroxide-induced apoptosis and necrosis. *Proc Natl Acad Sci U S A* 103: 1727-31,
19 2006.
- 20 24. Nakayama H, Chen X, Baines CP, Klevitsky R, Zhang X, Zhang H, Jaleel N, Chua BH, Hewett
21 TE, Robbins J, Houser SR, Molkentin JD. Ca²⁺- and mitochondrial-dependent cardiomyocyte
22 necrosis as a primary mediator of heart failure. *J Clin Invest* 117: 2431-44, 2007.
- 23 25. Nigmatullina RR, Kirillova VV, Jourjikiya RK, Mukhamedyarov MA, Kudrin VS, Klodt PM,
24 Palotas A. Disrupted Serotonergic and Sympathoadrenal Systems in Patients with Chronic Heart
25 Failure May Serve as New Therapeutic Targets and Novel Biomarkers to Assess Severity,
26 Progression and Response to Treatment. *Cardiology* 113: 277-286, 2009.
- 27 26. Pchejetski D, Kunduzova O, Dayon A, Calise D, Seguelas MH, Leducq N, Seif I, Parini A,
28 Cuvillier O. Oxidative stress-dependent sphingosine kinase-1 inhibition mediates monoamine
29 oxidase A-associated cardiac cell apoptosis. *Circ Res* 100: 41-9, 2007.
- 30 27. Pizzinat N, Marchal-Victorion S, Maurel A, Ordener C, Bompert G, Parini A. Substrate-
31 dependent regulation of MAO-A in rat mesangial cells: involvement of dopamine D2-like
32 receptors. *Am J Physiol Renal Physiol* 284: F167-74, 2003.
- 33 28. Rimbaud S, Garnier A, Ventura-Clapier R. Mitochondrial biogenesis in cardiac pathophysiology.
34 *Pharmacol Rep* 61: 131-8, 2009.
- 35 29. Rosca MG, Hoppel CL. Mitochondria in heart failure. *Cardiovasc Res* 88: 40-50.
- 36 30. Sahin E, Colla S, Liesa M, Moslehi J, Muller FL, Guo M, Cooper M, Kotton D, Fabian AJ,
37 Walkey C, Maser RS, Tonon G, Foerster F, Xiong R, Wang YA, Shukla SA, Jaskelioff M, Martin
38 ES, Heffernan TP, Protopopov A, Ivanova E, Mahoney JE, Kost-Alimova M, Perry SR, Bronson
39 R, Liao R, Mulligan R, Shirihai OS, Chin L, DePinho RA. Telomere dysfunction induces
40 metabolic and mitochondrial compromise. *Nature* 470: 359-65.
- 41 31. Sano M, Minamino T, Toko H, Miyauchi H, Orimo M, Qin Y, Akazawa H, Tateno K, Kayama Y,
42 Harada M, Shimizu I, Asahara T, Hamada H, Tomita S, Molkentin JD, Zou Y, Komuro I. p53-
43 induced inhibition of Hif-1 causes cardiac dysfunction during pressure overload. *Nature* 446:
44 444-8, 2007.
- 45 32. Sebastiani M, Giordano C, Nediani C, Travaglini C, Borchini E, Zani M, Feccia M, Mancini M,
46 Petrozza V, Cossarizza A, Gallo P, Taylor RW, d'Amati G. Induction of mitochondrial biogenesis
47 is a maladaptive mechanism in mitochondrial cardiomyopathies. *J. Am. Coll. Cardiol.* 50: 1362-
48 1369, 2007.
- 49 33. Toko H, Takahashi H, Kayama Y, Oka T, Minamino T, Okada S, Morimoto S, Zhan DY,
50 Terasaki F, Anderson ME, Inoue M, Yao A, Nagai R, Kitaura Y, Sasaguri T, Komuro I.
51 Ca²⁺/calmodulin-dependent kinase IIdelta causes heart failure by accumulation of p53 in dilated
52 cardiomyopathy. *Circulation* 122: 891-9.
- 53
54
55
56
57
58
59
60

Villeneuve

- 1
2
3 34. Tsutsui H, Kinugawa S, Matsushima S. Mitochondrial oxidative stress and dysfunction in
4 myocardial remodelling. *Cardiovasc Res* 81: 449-56, 2009.
5 35. Tu HC, Ren D, Wang GX, Chen DY, Westergard TD, Kim H, Sasagawa S, Hsieh JJ, Cheng EH.
6 The p53-cathepsin axis cooperates with ROS to activate programmed necrotic death upon DNA
7 damage. *Proc Natl Acad Sci U S A* 106: 1093-8, 2009.
8 36. Velez JM, Miriyala S, Nithipongvanitch R, Noel T, Plabplueng CD, Oberley T, Jungsuwadee P,
9 Van Remmen H, Vore M, St Clair DK. p53 Regulates oxidative stress-mediated retrograde
10 signaling: a novel mechanism for chemotherapy-induced cardiac injury. *PLoS One* 6: e18005.
11 37. Waters FJ, Shavlakadze T, McIldowie MJ, Piggott MJ, Grounds MD. Use of pifithrin to inhibit
12 p53-mediated signalling of TNF in dystrophic muscles of mdx mice. *Mol Cell Biochem* 337: 119-
13 31.
14 38. Zhang D, Mott JL, Farrar P, Ryerse JS, Chang SW, Stevens M, Denniger G, Zassenhaus HP.
15 Mitochondrial DNA mutations activate the mitochondrial apoptotic pathway and cause dilated
16 cardiomyopathy. *Cardiovasc Res* 57: 147-57, 2003.
17
18
19
20
21
22
23
24
25
26
27
28
29
30
31
32
33
34
35
36
37
38
39
40
41
42
43
44
45
46
47
48
49
50
51
52
53
54
55
56
57
58
59
60

Villeneuve

Table 1. Echocardiographic measurements of NTg and MAO-A Tg mice in control conditions and after chronic treatment with clorgyline

	Untreated				Clorgyline-treated		
	NTg	Tg-3 months	Tg-5 months	Tg-7 months	NTg	Tg-3 months	Tg-5 months
N° of animals	16	11	12	4	5	5	5
DSWT, mm	0.67±0.01	0.64±0.01	0.67±0.01	0.68±0.04	0.63±0.01	0.63±0.02	0.66±0.01
DPWT, mm	0.68±0.02	0.64±0.01	0.69±0.02	0.76±0.09	0.67±0.02	0.65±0.02	0.64±0.01
LVEDD, mm	3.84±0.03	4.40±0.09*	4.50±0.06*	4.88±0.26*	3.93±0.16	4.02±0.17	4.16±0.09
LVESD, mm	2.73±0.05	3.40±0.01*	3.63±0.09*	4.08±0.39*	2.74±0.17	2.92±0.18	3.12±0.07#
FS (%)	28.9±1.0	22.5±1.1*	19.4±1.2*	16.5±3.5*	30.5±2.7	27.1±1.7	25.3±0.7#
HR, bpm	444.4±12.9	475.0±12.5	457.2±17.0	484.8±30.5	406.5±20.7	453.0±29.1	449.5±8.9

Diastolic Septal Wall Thickness (DSWT), Diastolic Posterior Wall Thickness (DPWT), Left-Ventricular End-Diastolic Diameter (LVEDD), Left-Ventricular End-Systolic Diameter (LVESD), Fractional shortening (FS), and Heart Rate (HR) assessment by echocardiography. *p<0.05 in Tg vs NTg mice. #p<0.05 clorgyline-treated vs untreated age-matched Tg mice.

Villeneuve

Figure Legends

Figure 1. MAO-A activity is increased in response to hypertrophy, failure and aging in the heart. (A) MAO-A activity in cardiac homogenates from rats with ascendant aortic banding (Band) for 5 weeks (hypertrophy, n=5) or 15 weeks (HF, n=5) compared to age-matched sham (n=5). (B) MAO-A activity in cardiac homogenates from young (2 months), middle age (12 months) and senescent rats (24 months) (n=6). (C) MAO-A activity in isolated rat cardiomyocytes at the ages indicated (n=3-4). (*p<0.05, **p<0.01, ***p<0.001 vs indicated value).

Figure 2. MAO-A Tg mice overexpress an active MAO-A enzyme, specifically in cardiac mitochondria. (A) Cardiac MAO-A activity in NTg, Tg 61 and Tg 113 mice (n=3). The DNA transgene is represented above the histogram, with the α MHC promoter in front of the MAO-A cDNA. (B) Representative MAO-A immunoblot on cardiac and liver homogenates in NTg, Tg 61 and Tg 113 mice. (C) Double immunofluorescence staining on heart sections using MAO-A and Cox-IV antibodies (x 1000). (D) H₂O₂ measurements on isolated cardiac mitochondria incubated with tyramine (30 μ mol/L) and pargyline (100 μ mol/L) (n=4-5). (E) 5-HT, 5-HIAA, NE and DHPG contents in cardiac homogenates from NTg and Tg mice assessed with HPLC (n=5). (*p<0.05, ***p<0.001, §§§p<0.001 vs indicated value).

Figure 3. Evidences of cell death in the hearts of MAO-A Tg mice associated with reactive cellular hypertrophy and fibrosis. (A) Histological characterization (x 400) of ventricular pathology by hematoxylin-eosin (HE), periodic acid Schiff (PAS) and Green Masson's Trichrome staining in cardiac sections of NTg, Tg 61 and clorgyline-treated Tg 61 (Tg 61+clorg) mice at 5 months. Arrow indicates necrotic area. (B) Quantification of cardiomyocyte number per total area, cardiomyocyte diameter and collagen content on cardiac sections (n=5). (C) Evaluation of troponin-I levels by ELISA in plasma from NTg and Tg 61 mice at 1.5 and 3 months (n=4). (D) Quantification of TUNEL-positive apoptotic nuclei related to the total number of nuclei in cardiac sections from NTg and Tg 61 mice at 1.5 and 3 months (n=4). (E) Activated caspase-3 and (F) p53 immunoblots on heart homogenates from NTg and Tg 61 at 1.5 months. (*p<0.05, **p<0.01, ***p<0.001, §p<0.01, §§p<0.001 vs indicated value).

Villeneuve

Figure 4. Oxidative stress is increased in hearts from MAO-A overexpressing mice and participates in the development of dilated cardiomyopathy. (A) Real-time *in situ* measurements of H₂O₂ in ventricles from anesthetized Tg and NTg mice at 1.5 months (n=5) (B) 8-OH-dG immuno-histochemistry on cardiac sections from NTg, Tg 61 and clorgyline-treated Tg 61 (Tg 61+clorg) mice (x 400). Quantification of 8-OH-dG staining was expressed as percent of total area (n=5). (C) Activity of anti-oxidant enzymes glutathion peroxidase (GPX), catalase (CAT), and superoxide dismutase (Mn-SOD) in ventricles from 3 months old NTg and Tg 61 mice (n=5-6). (D) Fractional shortening (FS), Left-Ventricular Systolic Diameter (LVESD) and cardiomyocyte number in 5 months old NTg, Tg 61 untreated and N-acetylcystein-treated Tg 61 (Tg61 +NAC) mice (n=6). (*p<0.05, **p<0.01, ***p<0.001, §p<0.05, §§p<0.01, §§§p<0.001 vs indicated value).

Figure 5. MAO-A overexpression induces mitochondrial injury. (A) Geneset Enrichment Analysis for differentially expressed genes by microarray in Tg compared to NTg mice (2 months). Common themes were defined among the various overlapping and unique gene sets. Blue blocks and red blocks represent highly enriched in category among the various downregulated or upregulated genes, respectively. (B) Representative electron micrographs of ventricles from 1.5 months old NTg and Tg 61 mice (x 10000). Cardiomyocytes from Tg mice show electron-lucent areas in mitochondrial matrix (arrows) or concentric cristae (asterisk). (C) ATP concentrations in ventricle homogenates at 1.5 months (n=4). (D) Real-time RT-PCR expression of PGC-1 α mRNA at 2 months (n=5). (*p<0.05, **p<0.01 vs indicated value).

Figure 6. p53 mediates MAO-A-dependent cardiomyocyte necrosis. In (A, B and C), neonatal cardiomyocytes were untransduced (MOI 0) or transduced with AdeMAO-A at MOI 5. (A) Quantification of MAO-A activity by luminescence (n=3). (B), LDH release following treatment with 50 μ mol/L NE for 24 hours (n=8-9). (C), LDH release in response to 500 μ mol/L Tyr for 24 hours in the presence of 10 μ mol/L clorgyline (Tyr+clorg) or 5 mmol/L NAC (Tyr+NAC), when indicated (n=4-5). (D), Analysis of total or phosphor(ser15)-p53 levels by immunoblot in AdeMAO-A-transduced neonatal cardiomyocytes (MOI 5) stimulated with 500 μ mol/L Tyr for the indicated time, (E) in the presence of NAC when indicated (n=3-5). GAPDH was used as a loading control. (F) LDH release in AdeMAO-A-transduced

Villeneuve

1
2
3 cardiomyocytes (MOI 5) transfected with Scr or p53 siRNA for 48 hours, and stimulated with 500
4 $\mu\text{mol/L}$ Tyr for 24 hours (n=7). Immunoblot illustrates silencing of p53 protein at 48 and 72 hours
5
6 following siRNA transfection. (G) LDH release in AdeMAO-A-transduced cardiomyocytes (MOI 5)
7
8 stimulated with 500 $\mu\text{mol/L}$ Tyr for 24 hours in the presence of 20 $\mu\text{mol/L}$ pifithrin, when indicated (n=6-
9
10
11 8). *p<0.05, **p<0.01, ***p<0.001, §p<0.05, §§p<0.01 vs indicated values or Ct.

12
13
14 **Figure 7.** p53 mediates mitochondrial injury and PGC-1 α repression induced by MAO-A activation in
15
16 neonatal cardiomyocytes transduced with AdeMAO-A (MOI 5). (A) Representative electron micrographs
17
18 of cardiomyocytes transfected with Scr or p53 siRNA and stimulated with Tyr for 4 hours (Tyr) (x35000).
19
20 Tyr-treated Scr-transfected cardiomyocytes display damaged mitochondria (arrows). (B) Kinetics of ATP
21
22 content in AdeMAO-A-transduced cardiomyocytes (MOI 5) treated with Tyr (n=3) compared to
23
24 untransduced (MOI 0) cells. (C) PGC-1 α expression by real-time RT-PCR in cardiomyocytes transfected
25
26 with Scr or p53 siRNA and stimulated with Tyr for 4 hours (n=8). (D) LDH release in cardiomyocytes co-
27
28 infected or not with AdePGC-1 α , and stimulated with Tyr for 24 hours (n=4). (E) Schematic
29
30 representation of MAO-A induced necrosis signalling pathway in cardiomyocytes. **p<0.01,
31
32 ***p<0.001, §p<0.05 vs indicated values.
33
34
35
36
37
38
39
40
41
42
43
44
45
46
47
48
49
50
51
52
53
54
55
56
57
58
59
60

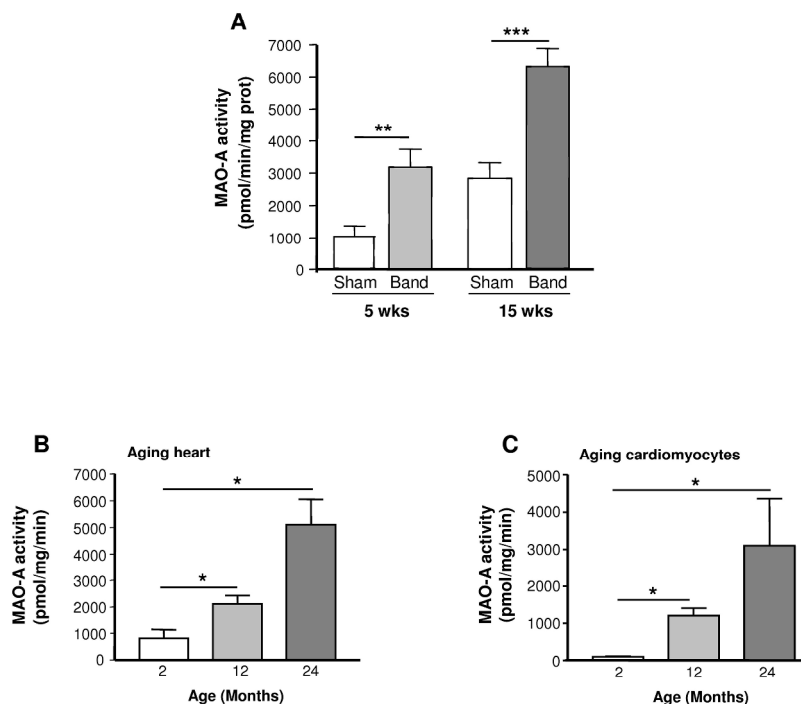


Fig.1: MAO-A activity is increased in response to hypertrophy, failure and aging in the heart. (A) MAO-A activity in cardiac homogenates from rats with ascendant aortic banding (Band) for 5 weeks (hypertrophy, n=5) or 15 weeks (heart failure, n=5) compared to age-matched sham (n=5). (B) MAO-A activity in cardiac homogenates from young (2 months), middle age (12 months) and senescent rats (24 months) (n=6). (C) MAO-A activity in isolated rat cardiomyocytes at the ages indicated (n=3-4). (*p<0.05, **p<0.01, ***p<0.001 vs indicated value).
253x337mm (300 x 300 DPI)

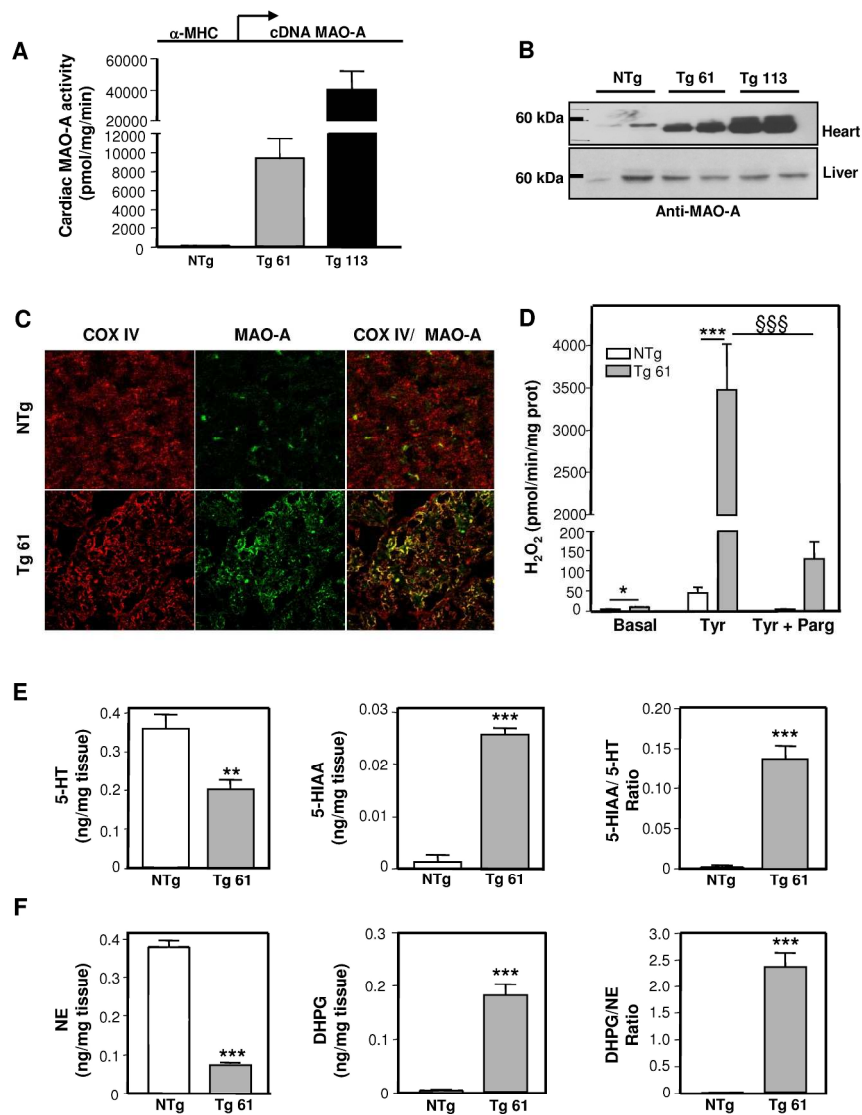


Fig. 2: MAO-A Tg mice overexpress an active MAO-A enzyme, specifically in cardiac mitochondria. (A) Cardiac MAO-A activity in NTg, Tg 61 and Tg 113 mice (n=3). The DNA transgene is represented above the histogram, with the αMHC promoter in front of the MAO-A cDNA. (B) Representative MAO-A immunoblot on cardiac and liver homogenates in NTg, Tg 61 and Tg 113 mice. (C) Double immunofluorescence staining on heart sections using MAO-A and Cox-IV antibodies (x 1000). (D) H₂O₂ measurements on isolated cardiac mitochondria incubated with tyramine (30 μmol/L) and pargyline (100 μmol/L) (n=4-5). (E) 5-HT, 5-HIAA, NE and DHPG contents in cardiac homogenates from NTg and Tg mice assessed with HPLC (n=5). (*p<0.05, ***p<0.001, §§§p<0.001 vs indicated value)

253x337mm (300 x 300 DPI)

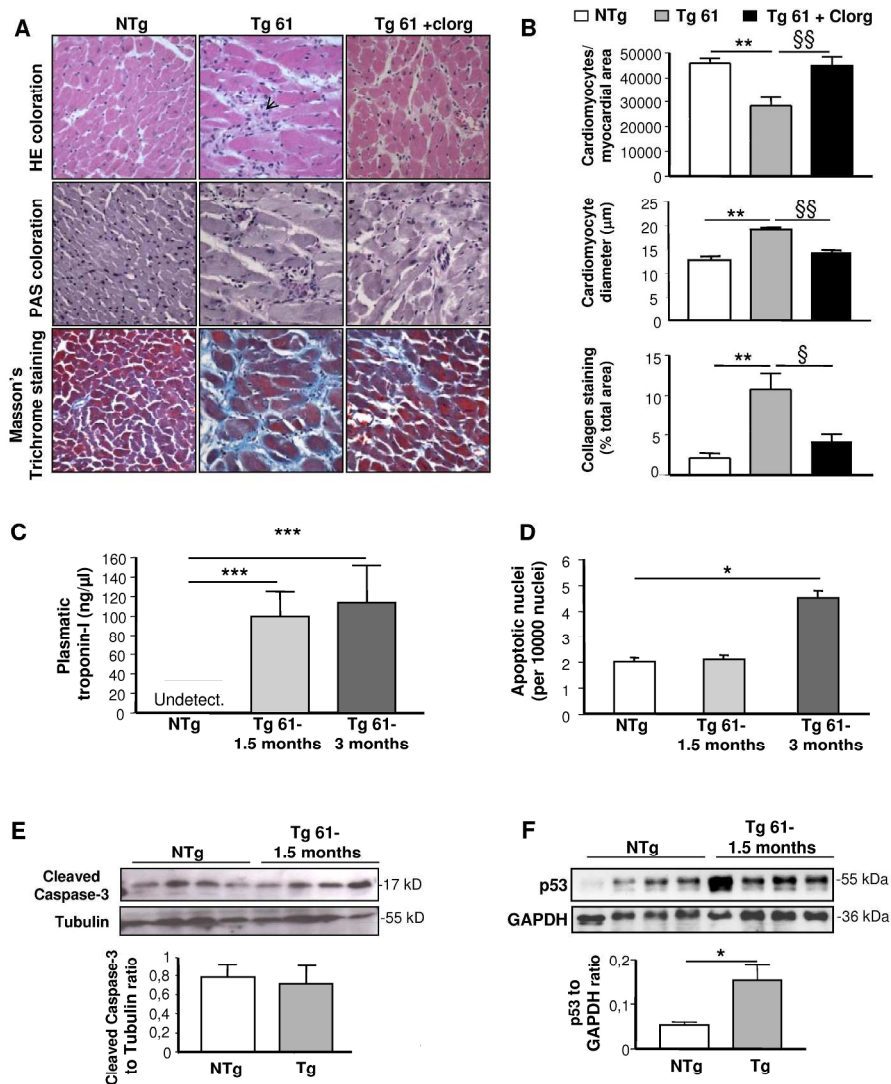


Fig. 3: Evidences of cell death in the hearts of MAO-A Tg mice associated with reactive cellular hypertrophy and fibrosis. (A) Histological characterization (x 400) of ventricular pathology by hematoxylin-eosin (HE), periodic acid Schiff (PAS) and Green Masson's Trichrome staining in cardiac sections of NTg, Tg 61 and clorgyline-treated Tg 61 (Tg 61+clorg) mice at 5 months. Arrow indicates necrotic area. (B) Quantification of cardiomyocyte number per total area, cardiomyocyte diameter and collagen content on cardiac sections (n=5). (C) Evaluation of troponin-I levels by ELISA in plasma from NTg and Tg 61 mice at 1.5 and 3 months (n=4). (D) Quantification of TUNEL-positive apoptotic nuclei related to the total number of nuclei in cardiac sections from NTg and Tg 61 mice at 1.5 and 3 months (n=4). (E) Activated caspase-3 and (F) p53 immunoblots on heart homogenates from NTg and Tg 61 at 1.5 months. (*p<0.05, **p<0.01, ***p<0.001, §p<0.01, §§p<0.001 vs indicated value).
253x337mm (300 x 300 DPI)

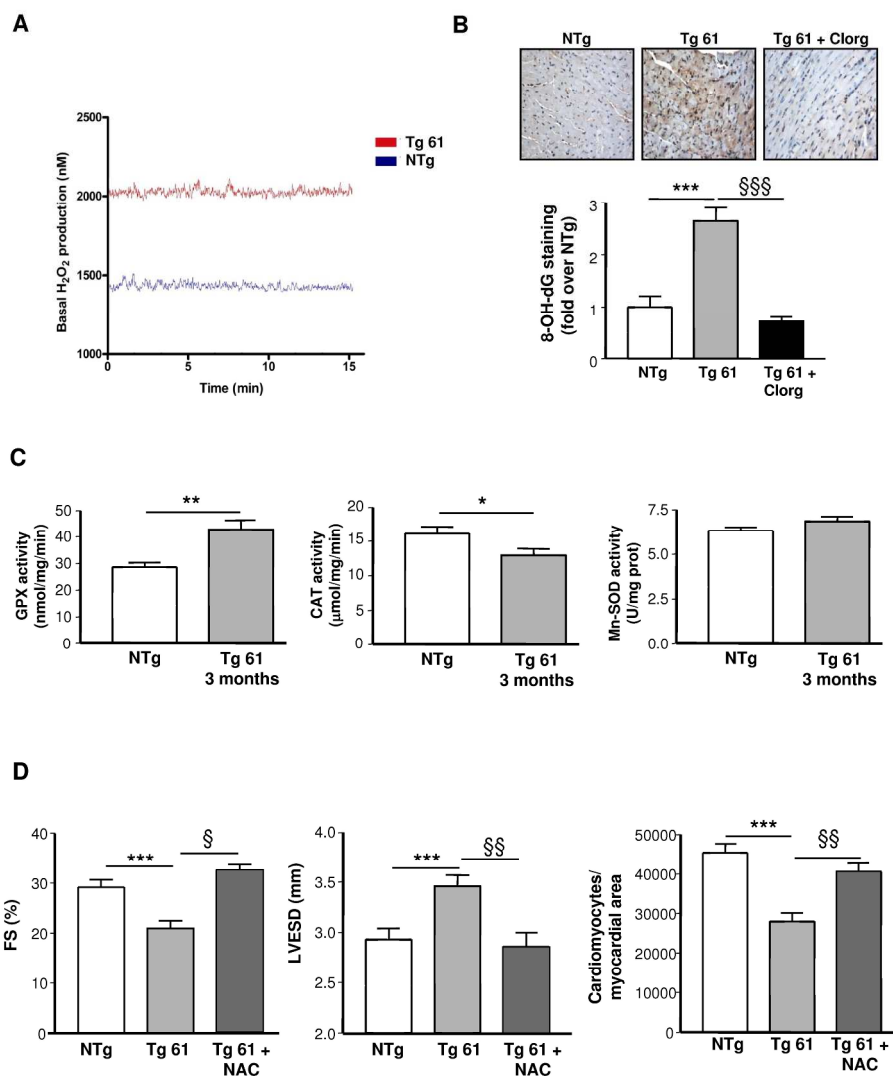


Figure 4. Oxidative stress is increased in hearts from MAO-A overexpressing mice and participates in the development of dilated cardiomyopathy. (A) Real-time in situ measurements of H₂O₂ in ventricles from anesthetized Tg and NTg mice at 1.5 months (n=5) (B) 8-OH-dG immuno-histochemistry on cardiac sections from NTg, Tg 61 and clorgyline-treated Tg 61 (Tg 61+clorg) mice (x 400). Quantification of 8-OH-dG staining was expressed as percent of total area (n=5). (C) Activity of anti-oxidant enzymes glutathion peroxidase (GPX), catalase (CAT), and superoxide dismutase (Mn-SOD) in ventricles from 3 months old NTg and Tg 61 mice (n=5-6). (D) Fractional shortening (FS), Left-Ventricular Systolic Diameter (LVESD) and cardiomyocyte number in 5 months old NTg, Tg 61 untreated and N-acetyl-cystein-treated Tg 61 (Tg61+NAC) mice (n=6). (*p<0.05, **p<0.01, ***p<0.001, §p<0.05, §§p<0.01, §§§p<0.001 vs indicated value).

253x337mm (300 x 300 DPI)

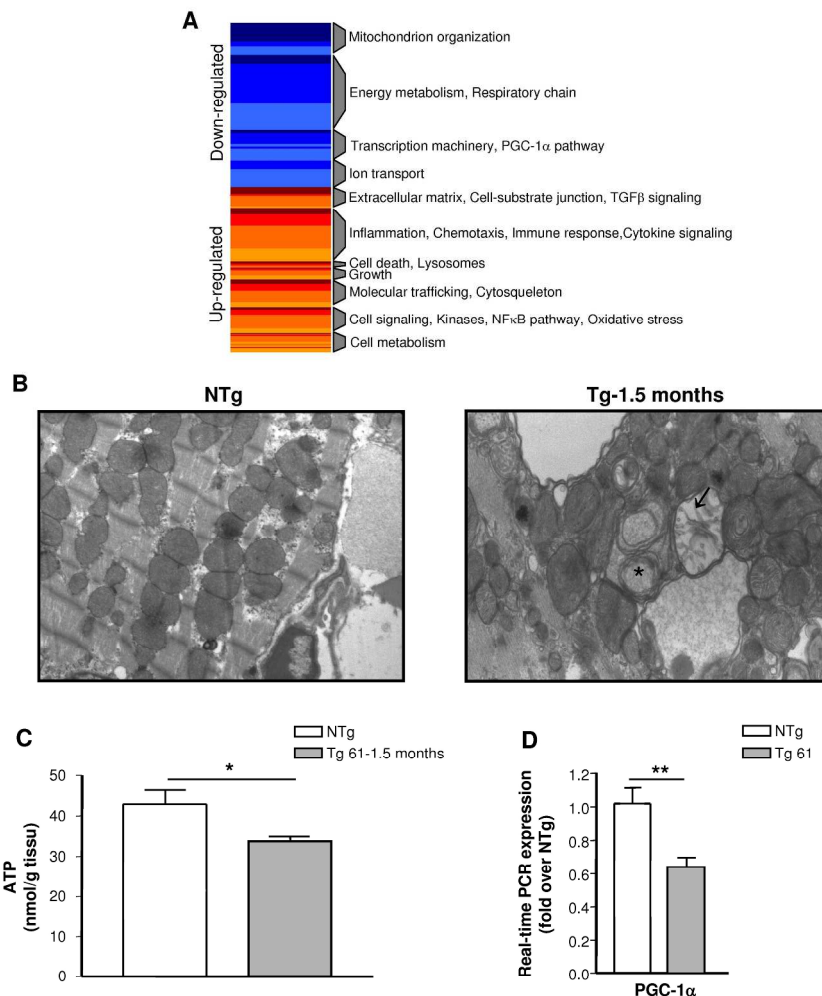


Fig. 5: MAO-A overexpression induces mitochondrial injury. (A) Geneset Enrichment Analysis for differentially expressed genes by microarray in Tg compared to NTg mice (2 months). Common themes were defined among the various overlapping and unique gene sets. Blue blocks and red blocks represent highly enriched in category among the various downregulated or upregulated genes, respectively. (B) Representative electron micrographs of ventricles from 1.5 months old NTg and Tg 61 mice (x 10000). Cardiomyocytes from Tg mice show electron-lucent areas in mitochondrial matrix (arrows) or concentric cristae (asterisk). (C) ATP concentrations in ventricle homogenates at 1.5 months (n=4). (D) Real-time RT-PCR expression of PGC-1 α mRNA at 2 months (n=5). (* p <0.05, ** p <0.01 vs indicated value).
253x337mm (300 x 300 DPI)

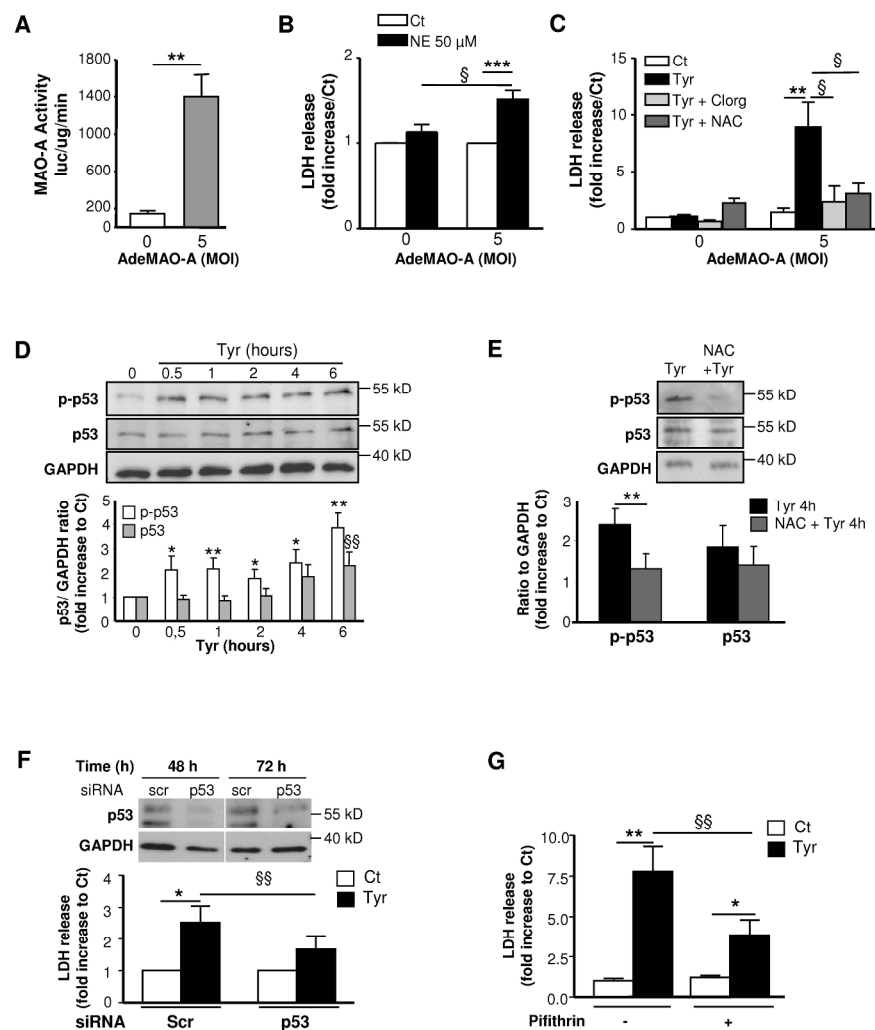


Fig. 6: p53 mediates MAO-A-dependent cardiomyocyte necrosis. In (A, B and C), neonatal cardiomyocytes were untransduced (MOI 0) or transduced with AdeMAO-A at MOI 5. (A) Quantification of MAO-A activity by luminescence (n=3). (B), LDH release following treatment with 50 μmol/L NE for 24 hours (n=8-9). (C), LDH release in response to 500 μmol/L Tyr for 24 hours in the presence of 10 μmol/L clorgyline (Tyr+clorg) or 5 mmol/L NAC (Tyr+NAC), when indicated (n=4-5). (D), Analysis of total or phosphor(ser15)-p53 levels by immunoblot in AdeMAO-A-transduced neonatal cardiomyocytes (MOI 5) stimulated with 500 μmol/L Tyr for the indicated time, (E) in the presence of NAC when indicated (n=3-5). GAPDH was used as a loading control. (F) LDH release in AdeMAO-A-transduced cardiomyocytes (MOI 5) transfected with Scr or p53 siRNA for 48 hours, and stimulated with 500 μmol/L Tyr for 24 hours (n=7). Immunoblot illustrates silencing of p53 protein at 48 and 72 hours following siRNA transfection. (G) LDH release in AdeMAO-A-transduced cardiomyocytes (MOI 5) stimulated with 500 μmol/L Tyr for 24 hours in the presence of 20 μmol/L pifithrin, when indicated (n=6-8). *p<0.05, **p<0.01, ***p<0.001, §p<0.05, §§p<0.01 vs indicated values or Ct. 253x337mm (300 x 300 DPI)

1
2
3
4
5
6
7
8
9
10
11
12
13
14
15
16
17
18
19
20
21
22
23
24
25
26
27
28
29
30
31
32
33
34
35
36
37
38
39
40
41
42
43
44
45
46
47
48
49
50
51
52
53
54
55
56
57
58
59
60

CONFIDENTIAL - For Peer Review only

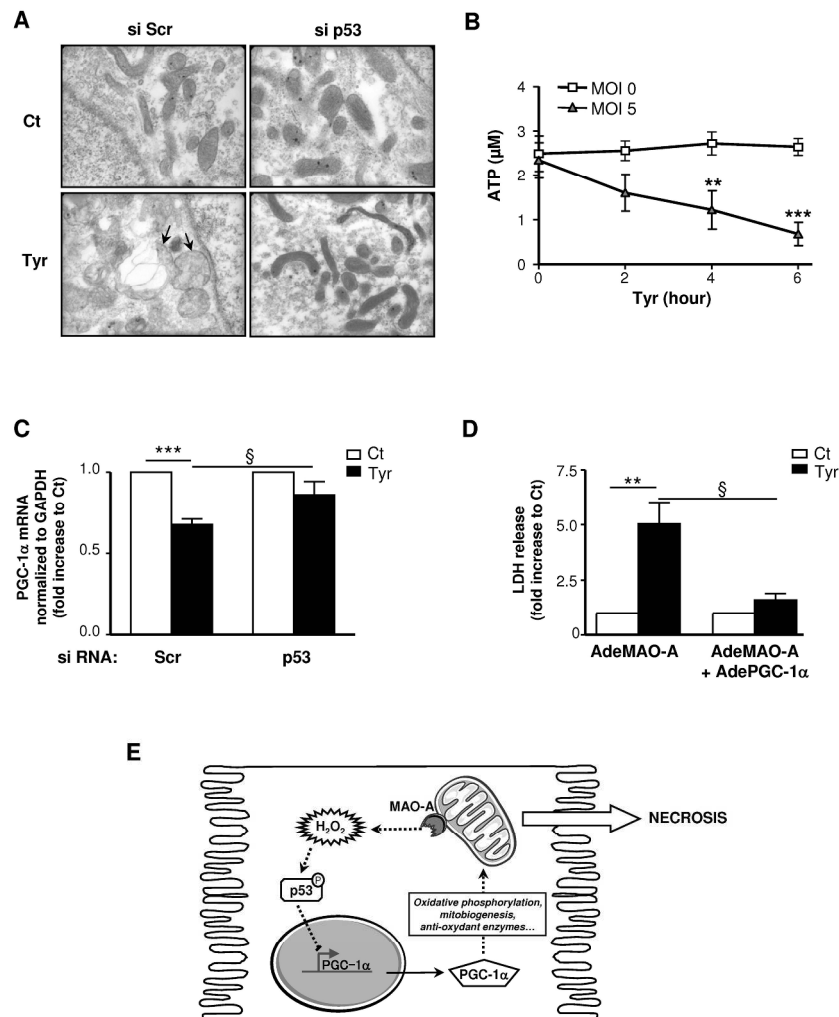


Fig. 7: p3 mediates mitochondrial injury and PGC-1α repression induced by MAO-A activation in neonatal cardiomyocytes transduced with AdeMAO-A (MOI 5). (A) Representative electron micrographs of cardiomyocytes transfected with Scr or p53 siRNA and stimulated with Tyr for 4 hours (Tyr) (x35000). Tyr-treated Scr-transfected cardiomyocytes display damaged mitochondria (arrows). (B) Kinetics of ATP content in AdeMAO-A-transduced cardiomyocytes (MOI 5) treated with Tyr (n=3) compared to untransduced (MOI 0) cells. (C) PGC-1α expression by real-time RT-PCR in cardiomyocytes transfected with Scr or p53 siRNA and stimulated with Tyr for 4 hours (n=8). (D) LDH release in cardiomyocytes co-infected or not with AdePGC-1α, and stimulated with Tyr for 24 hours (n=4). (E) Schematic representation of MAO-A induced necrosis signalling pathway in cardiomyocytes. **p<0.01, ***p<0.001, §p<0.05 vs indicated values.

253x337mm (300 x 300 DPI)

Villeneuve et al.

Supplemental legends

Supplemental Figure 1. MAO-A cardiac overexpression triggers mice premature death.

Kaplan-Meier analysis of death with aging in NTg (n=26), Tg 61 (n=38) and Tg 113 mice (n=17).

Supplemental Figure 2. MAO-A transgenic line 113 develops dilated cardiomyopathy and heart failure with cardiomyocytes loss and compensative hypertrophy and fibrosis.

(A) Fractional shortening (FS) and left-ventricular diastolic diameter (LVEDD) assessment by echocardiography in 2 months-old Ntg or Tg 113 mice (n=2-6). (**p<0.001 vs NTg). (B) Histological characterization (x 400) of ventricular pathology by hematoxylin-eosin (HE), periodic acid Schiff (PAS) and Masson's trichrome (green) staining in cardiac sections of NTg and Tg 113 at 2 months. Arrow indicates necrotic area. (C) Quantification of cardiomyocyte number per total area (n=4), cardiomyocyte diameter (n=4) and collagen content on cardiac sections (n=4) (*p<0.05, **p<0.01 or ***p<0.001 vs Ntg).

Supplemental Figure 3. Transcriptome analysis in MAO-A overexpressing mice at the ages of 1.5 and 3 months.

Expression of genes involved in inflammation (A), cardiac remodelling (B) and cardiac fibrosis (C). Expression of the gene of interest is normalized to the expression of 3 housekeeping genes and results are expressed as fold over NTg mice (n=4). (*p<0.05 vs NTg).

MCP1: Monocyte chemoattractant protein 1 (Ccl2), IL6: Interleukin 6, TNFa: Tumor necrosis factor alpha, aSkact: Squeletal alpha actin, aMHC: Myosin heavy chain alpha, bMHC: Myosin heavy chain beta, ANP: Atrial natriuretic peptide, BNP: B-type natriuretic peptide, SERCA: sarco/endoplasmic reticulum calcium ATPase, Coll1a1: Collagen type I alpha 1, Col3a1: Collagen type III alpha 1, Fn1: Fibronectin 1, Mmp9: Matrix metalloprotease 9, Vim: Vimentin

Supplemental Figure 4. MAO-A overexpression triggers increased ROS production in neonatal cardiomyocytes stimulated with tyramine.

ROS generation in cardiomyocytes transduced with AdeMAO-A (MOI 5) or untransduced (MOI 0) and treated with 500 µmol/L Tyr for 2 hours. Tyr stimulation was performed in the presence of NAC (5 mmol/L) or clorgyline (10 µmol/L), when indicated (n=9) (*p<0.05, §p<0.05 and ##p<0.01 vs indicated value).

Villeneuve et al.

Supplemental Tables

Table 1: Up-regulated genes encoding mitochondrial proteins

Symbol	Protein name	Accession number	Fold over NTg	p value
TSPO	translocator protein (18kDa)	P222657	2,26	7,30E-09
HCLS1	hematopoietic cell-specific Lyn substrate 1	P297679	2,22	5,70E-07
MTCH1	mitochondrial carrier homolog 1 (C. elegans)	P458242	2,19	1,13E-04
UCP2	uncoupling protein 2 (mitochondrial, proton carrier)	P297105	2,07	2,58E-05
CYBB	cytochrome b-245, beta polypeptide	P444628	1,99	6,30E-08
RAB32	RAB32, member RAS oncogene family	P293688	1,97	4,69E-08
SLC25A45	solute carrier family 25, member 45	P349727	1,92	1,64E-07
GPRC5C	G protein-coupled receptor, family C, group 5,	P309988	1,85	4,54E-06
ASS1	argininosuccinate synthetase 1	P361165	1,85	1,77E-06
GPX1	glutathione peroxidase 1	P684378	1,78	1,59E-06
SLC25A1	solute carrier family 25 (mitochondrial carrier; citrate transporter), member 1	P350922	1,77	1,79E-06
GRN	granulin	P192800	1,75	3,94E-05
PISD	phosphatidylserine decarboxylase	P422338	1,69	3,28E-05
VARS	valyl-tRNA synthetase	P203501	1,69	1,12E-04
PRELID1	PRELI domain containing 1	P505337	1,67	3,15E-06
SARDH	sarcosine dehydrogenase	P492676	1,67	1,31E-04
CPT1C	carnitine palmitoyltransferase 1C	P269942	1,64	9,29E-07
RNASEL	ribonuclease L (2',5'-oligoadenylate synthetase-dependent)	P377760	1,62	9,56E-07
PRDX4	peroxiredoxin 4	P200819	1,62	1,61E-06
HK1	hexokinase 1	P479599	1,60	2,66E-03
CKB	creatine kinase, brain	P425772	1,57	1,56E-03
SFXN1	sideroflexin 1	P418526	1,55	2,90E-07
PYCR1	pyrroline-5-carboxylate reductase 1	P503896	1,54	2,48E-05
TK2	thymidine kinase 2, mitochondrial	P310398	1,50	7,31E-05
CYB5R3	cytochrome b5 reductase 3	P153170	1,48	1,19E-03
CYBA	cytochrome b-245, alpha polypeptide	P131800	1,47	1,92E-03
SLC25A10	solute carrier family 25 (mitochondrial carrier; dicarboxylate transporter), member 10	P404904	1,43	1,39E-03
STAR	steroidogenic acute regulatory protein	P274436	1,42	3,04E-04

Table 2: Down-regulated genes encoding mitochondrial proteins

Symbol	Protein name	Accession number	Fold over NTg	p value
MRPS33	mitochondrial ribosomal protein S33	P342896	0,37	1,29E-06
LAP3	leucine aminopeptidase 3	P431662	0,38	8,45E-06
MRPS18C	mitochondrial ribosomal protein S18C	P108484	0,39	1,99E-07
MRPL1	mitochondrial ribosomal protein L1	P86073	0,39	7,22E-08
PITRM1	pitrilysin metalloproteinase 1	P474960	0,39	9,45E-07
PPM1K	protein phosphatase 1K (PP2C domain containing)	P265219	0,40	2,52E-07
PDK4	pyruvate dehydrogenase kinase, isozyme 4	P350453	0,40	8,20E-05
DBT	dihydrolipoamide branched chain transacylase E2	P569348	0,42	3,90E-08
SH3GLB1	SH3-domain GRB2-like endophilin B1	P32249	0,43	6,40E-06

Villeneuve et al.

1					
2					
3	MLYCD	malonyl-CoA decarboxylase	P222283	0,43	9,04E-09
4	MCEE	methylmalonyl CoA epimerase	P320481	0,43	2,07E-06
5	TFB2M	transcription factor B2, mitochondrial	P374499	0,45	1,52E-05
6	UCP3	uncoupling protein 3 (mitochondrial, proton carrier)	P380379	0,45	1,25E-04
7	ND4L	NADH dehydrogenase, subunit 4L (complex I)	P245525	0,45	7,44E-05
8	MAOB	monoamine oxidase B	P302566	0,48	1,00E-05
9					
10	COX16	COX16 cytochrome c oxidase assembly homolog (S. cerevisiae)	P404300	0,49	1,07E-06
11	ATP5F1	ATP synthase, H ⁺ transporting, mitochondrial F0 complex, subunit B1	P106929	0,50	6,53E-04
12					
13	MRPL47	mitochondrial ribosomal protein L47	P302291	0,50	7,80E-09
14	MRPS35	mitochondrial ribosomal protein S35	P110841	0,51	7,67E-09
15	CPOX	coproporphyrinogen oxidase	P257258	0,51	3,10E-05
16	HSDL2	hydroxysteroid dehydrogenase like 2	P281930	0,51	1,24E-07
17	MRPS25	mitochondrial ribosomal protein S25	P121325	0,51	2,63E-07
18	ACSS1	acyl-CoA synthetase short-chain family member 1	P479321	0,51	1,67E-06
19	PINK1	PTEN induced putative kinase 1	P196605	0,51	7,29E-07
20	C5ORF33	chromosome 5 open reading frame 33	P243323	0,52	1,13E-06
21	DECR1	2,4-dienoyl CoA reductase 1, mitochondrial	P208555	0,52	1,57E-06
22					
23	CHCHD3	coiled-coil-helix-coiled-coil-helix domain containing 3	P526335	0,52	8,93E-04
24	MTRF1	mitochondrial fission regulator 1	P143002	0,55	9,63E-07
25	MRPS22	mitochondrial ribosomal protein S22	P362903	0,55	6,63E-06
26	SLC25A46	solute carrier family 25, member 46	P176711	0,55	1,14E-05
27					
28	MRS2	MRS2 magnesium homeostasis factor homolog (S. cerevisiae)	P618187	0,55	5,91E-06
29					
30	AUH	AU RNA binding protein/enoyl-Coenzyme A hydratase	P372473	0,55	9,13E-07
31					
32	NDUFB11	NADH dehydrogenase (ubiquinone) 1 beta subcomplex, 11, 17.3kDa	P205573	0,55	5,04E-05
33	DARS2	aspartyl-tRNA synthetase 2, mitochondrial	P102559	0,55	1,06E-08
34	SLC25A36	solute carrier family 25, member 36	P124121	0,56	1,83E-04
35	PDHA1	pyruvate dehydrogenase (lipoamide) alpha 1	P581435	0,56	6,01E-06
36	COQ7	coenzyme Q7 homolog, ubiquinone (yeast)	P161691	0,56	1,39E-07
37	NNT	nicotinamide nucleotide transhydrogenase	P113395	0,56	4,98E-06
38	MARCH5	membrane-associated ring finger (C3HC4) 5	P405668	0,56	2,00E-07
39					
40	COX7A2	cytochrome c oxidase subunit VIIa polypeptide 2 (liver)	P319031	0,56	2,50E-05
41					
42	NDUFA6	NADH dehydrogenase (ubiquinone) 1 alpha subcomplex, 6, 14kDa	P217474	0,57	2,89E-07
43	PDHX	pyruvate dehydrogenase complex, component X	P149946	0,57	1,34E-04
44	MFN1	mitofusin 1	P2732	0,57	5,50E-08
45	ADH5	alcohol dehydrogenase 5 (class III), chi polypeptide	P404275	0,57	3,60E-06
46	YARS2	tyrosyl-tRNA synthetase 2, mitochondrial	P373609	0,58	4,37E-07
47	MUT	methylmalonyl Coenzyme A mutase	P633163	0,58	7,62E-06
48	MRPS21	mitochondrial ribosomal protein S21	P509012	0,58	1,96E-06
49					
50	NDUFS6	NADH dehydrogenase (ubiquinone) Fe-S protein 6, 13kDa (NADH-coenzyme Q reductase)	P335077	0,58	4,48E-08
51					
52	SLC25A11	solute carrier family 25 (mitochondrial carrier; oxoglutarate carrier), member 11	P267454	0,58	7,32E-06
53					
54	TOMM7	translocase of outer mitochondrial membrane 7 homolog (yeast)	P206547	0,58	5,44E-05
55					
56	COX15	COX15 homolog, cytochrome c oxidase assembly protein (yeast)	P354744	0,58	6,47E-04
57					
58					
59					
60					

Villeneuve et al.

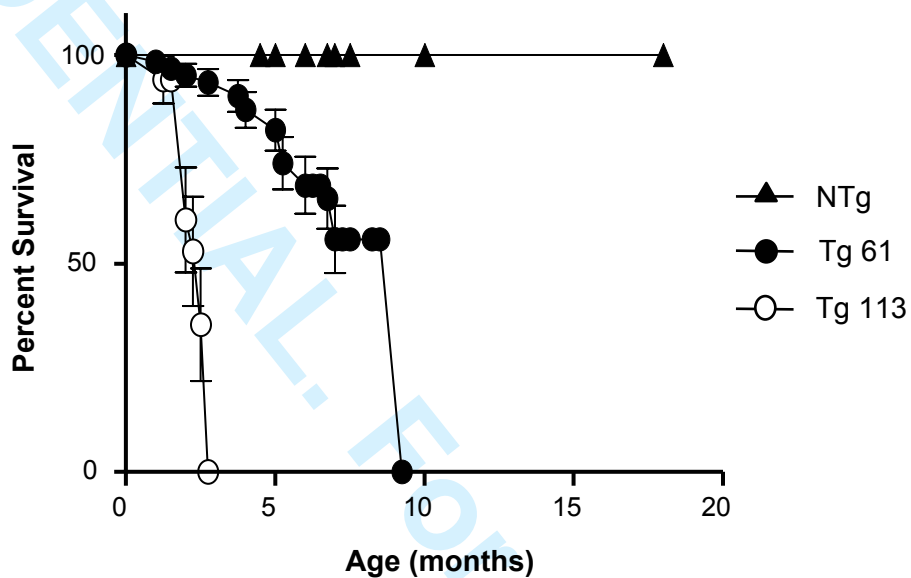
1				
2				
3		translocase of inner mitochondrial membrane 8		
4	TIMM8A	homolog A (yeast)	P373043	0,59 4,87E-07
5	DUT	deoxyuridine triphosphatase	P480360	0,59 8,03E-04
6	LYPLA1	lysophospholipase I	P8227	0,59 3,20E-05
7	MRPL22	mitochondrial ribosomal protein L22	P322994	0,59 9,60E-07
8	CLPX	ClpX caseinolytic peptidase X homolog (E. coli)	P304683	0,59 3,40E-05
9	MTERFD3	MTERF domain containing 3	P202623	0,60 2,05E-05
10	NDUFA8	NADH dehydrogenase (ubiquinone) 1 alpha		
11		subcomplex, 8, 19kDa	P475501	0,60 3,78E-03
12	PHB	prohibitin	P165934	0,60 6,26E-06
13	KIAA0564	KIAA0564	P221144	0,60 1,07E-04
14	SUCLA2	succinate-CoA ligase, ADP-forming, beta subunit	P111554	0,60 5,00E-05
15	FECH	ferrochelatase (protoporphyrin)	P266763	0,60 2,51E-04
16	NDUFA12	NADH dehydrogenase (ubiquinone) 1 alpha		
17		subcomplex, 12	P458540	0,60 1,73E-04
18	COX7B	cytochrome c oxidase subunit VIIb	P160664	0,61 1,11E-05
19	MRPL19	mitochondrial ribosomal protein L19	P604526	0,61 4,45E-07
20	ADHFE1	alcohol dehydrogenase, iron containing, 1	P116264	0,61 1,08E-04
21	UQCRH	ubiquinol-cytochrome c reductase hinge protein	P350301	0,61 4,20E-05
22	ATP5G3	ATP synthase, H ⁺ transporting, mitochondrial F0		
23		complex, subunit C3 (subunit 9)	P294849	0,61 5,88E-06
24	MTERFD1	MTERF domain containing 1	P507204	0,62 3,94E-04
25	SYNJ2BP	synaptojanin 2 binding protein	P662001	0,62 5,12E-04
26	ACOT2	acyl-CoA thioesterase 2	P525183	0,62 2,53E-04
27	SLC25A37	solute carrier family 25, member 37	P343429	0,62 4,87E-04
28	ATP5S	ATP synthase, H ⁺ transporting, mitochondrial F0		
29		complex, subunit s (factor B)	P195798	0,62 1,28E-06
30	RAB11FIP5	RAB11 family interacting protein 5 (class I)	P529360	0,62 2,83E-05
31	OXCT1	3-oxoacid CoA transferase 1	P107321	0,62 7,76E-07
32	SDHA	succinate dehydrogenase complex, subunit A,		
33		flavoprotein (Fp)	P458708	0,62 3,51E-03
34	COX7A2L	cytochrome c oxidase subunit VIIa polypeptide 2 like	P434803	0,62 2,19E-06
35	L2HGDH	L-2-hydroxyglutarate dehydrogenase	P221132	0,62 2,57E-05
36	ETFHDH	electron-transferring-flavoprotein dehydrogenase	P161574	0,62 2,21E-04
37	SLC25A26	solute carrier family 25, member 26	P71544	0,62 1,35E-06
38	TOMM20	translocase of outer mitochondrial membrane 20		
39		homolog (yeast)	P310930	0,62 1,82E-07
40	C18ORF55	chromosome 18 open reading frame 55	P395842	0,62 5,85E-06
41	YWHAZ	tyrosine 3-monooxygenase/tryptophan 5-		
42		monooxygenase activation protein, zeta polypeptide	P480709	0,63 1,65E-03
43	ACSL1	acyl-CoA synthetase long-chain family member 1	P496432	0,63 9,37E-05
44	PTPMT1	protein tyrosine phosphatase, mitochondrial 1	P226341	0,63 4,09E-08
45	SLC25A16	solute carrier family 25 (mitochondrial carrier;		
46		Graves disease autoantigen), member 16	P458870	0,63 6,08E-06
47	MRPL50	mitochondrial ribosomal protein L50	P112677	0,63 2,35E-05
48	DLAT	dihydrolipoamide S-acetyltransferase	P265106	0,63 2,05E-05
49	MCAT	malonyl CoA:ACP acyltransferase (mitochondrial)	P314855	0,63 3,36E-05
50	AFG3L1	AFG3 ATPase family gene 3-like 1 (S. cerevisiae)	P598714	0,64 4,11E-04
51	OGG1	8-oxoguanine DNA glycosylase	P489903	0,64 2,16E-03
52	ACSL6	acyl-CoA synthetase long-chain family member 6	P380699	0,64 9,22E-04
53	SSBP1	single-stranded DNA binding protein 1	P289685	0,64 4,11E-05
54	PPP1CC	protein phosphatase 1, catalytic subunit, gamma		
55		isoform	P519508	0,65 1,08E-04
56	NDUFV3	NADH dehydrogenase (ubiquinone) flavoprotein 3,	P170054	0,65 9,40E-06
57				
58				
59				
60				

Villeneuve et al.

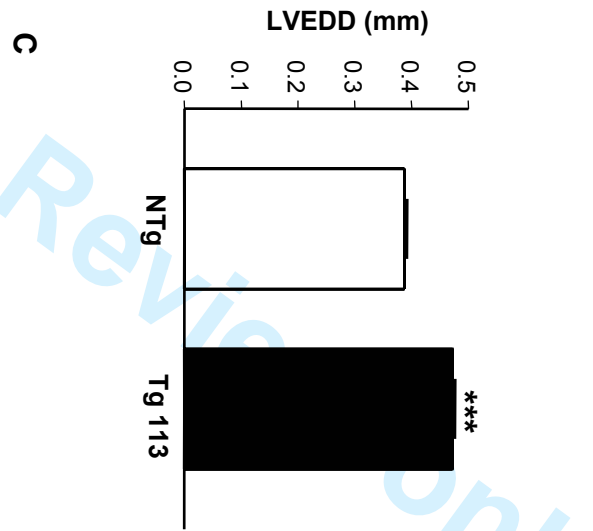
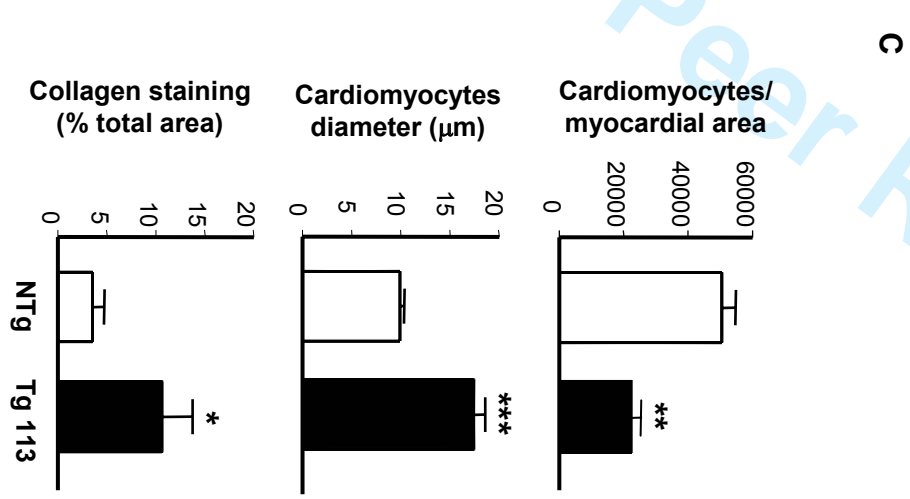
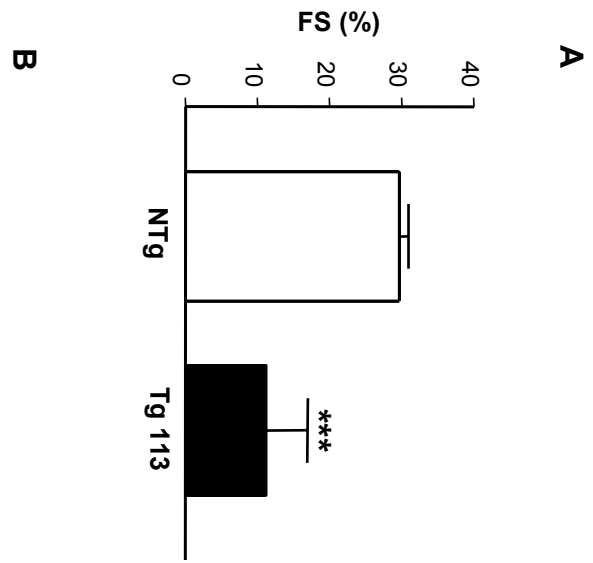
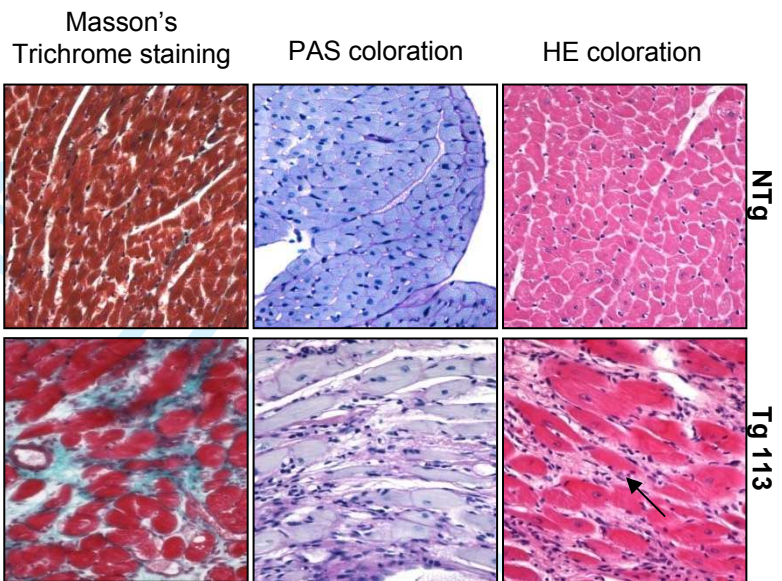
1				
2				
3		10kDa		
4	OXSM	3-oxoacyl-ACP synthase, mitochondrial	P312748	0,65 2,31E-05
5	SLC25A12	solute carrier family 25 (mitochondrial carrier, Aralar), member 12	P1196751	0,65 1,32E-03
6	MTRF1L	mitochondrial translational release factor 1-like	P397548	0,65 2,98E-08
7	MRPL40	mitochondrial ribosomal protein L40	P420627	0,65 4,15E-05
8	REEP1	receptor accessory protein 1	P508341	0,66 2,29E-06
9	SUOX	sulfite oxidase	P249360	0,66 1,20E-04
10	IMMP1L	IMP1 inner mitochondrial membrane peptidase-like (S. cerevisiae)	P3754	0,66 1,30E-04
11	PACS2	phosphofurin acidic cluster sorting protein 2	P439520	0,66 6,59E-07
12	MTIF2	mitochondrial translational initiation factor 2	P455597	0,66 3,67E-05
13	TOMM22	translocase of outer mitochondrial membrane 22 homolog (yeast)	P105339	0,66 1,86E-06
14	COX11	COX11 homolog, cytochrome c oxidase assembly protein (yeast)	P214319	0,66 3,00E-06
15	MRPL18	mitochondrial ribosomal protein L18	P210474	0,66 1,09E-03
16	CPT1B	carnitine palmitoyltransferase 1B (muscle)	P232913	0,66 2,28E-04
17	MCCC1	methylcrotonoyl-Coenzyme A carboxylase 1 (alpha)	P282975	0,66 3,81E-05
18	ACOT13	acyl-CoA thioesterase 13	P502422	0,67 8,22E-06
19	ATP5B	ATP synthase, H ⁺ transporting, mitochondrial F1 complex, beta polypeptide	P328078	0,67 2,13E-04
20	NDUFA4	NADH dehydrogenase (ubiquinone) 1 alpha subcomplex, 4, 9kDa	P552832	0,67 1,53E-05
21	CAPRN2	caprin family member 2	P204944	0,67 4,57E-05
22	MMADHC	methylmalonic aciduria (cobalamin deficiency) cblD type, with homocystinuria	P236721	0,67 2,31E-04
23	ABCD3	ATP-binding cassette, sub-family D (ALD), member 3	P394395	0,67 1,54E-05
24	USMG5	up-regulated during skeletal muscle growth 5 homolog (mouse)	P181365	0,68 3,78E-03
25	C2ORF56	chromosome 2 open reading frame 56	P180826	0,68 6,56E-07
26	ECSIT	ECSIT homolog (Drosophila)	P348548	0,68 3,94E-05
27	MRPL32	mitochondrial ribosomal protein L32	P141818	0,68 2,28E-04
28	BCAT2	branched chain aminotransferase 2, mitochondrial	P448266	0,68 3,65E-05
29	ECHDC3	enoyl Coenzyme A hydratase domain containing 3	P475378	0,68 1,14E-03
30	RNASET2	ribonuclease T2	P477019	0,68 8,88E-06
31	SLC25A33	solute carrier family 25, member 33	P156434	0,68 1,86E-03
32	SDHD	succinate dehydrogenase complex, subunit D, integral membrane protein	P260871	0,69 1,31E-05
33	MRPS31	mitochondrial ribosomal protein S31	P319732	0,69 2,80E-05
34	NDUFS8	NADH dehydrogenase (ubiquinone) Fe-S protein 8, 23kDa (NADH-coenzyme Q reductase)	P247441	0,69 6,35E-04
35	TUSC3	tumor suppressor candidate 3	P515347	0,69 1,32E-03
36	PARL	presenilin associated, rhomboid-like	P247943	0,69 5,87E-05
37	PDPR	pyruvate dehydrogenase phosphatase regulatory subunit	P137829	0,69 4,66E-04
38	ABCE1	ATP-binding cassette, sub-family E (OABP), member 1	P332822	0,69 9,62E-06
39	COX6B2	cytochrome c oxidase subunit VIb polypeptide 2 (testis)	P300506	0,69 3,58E-04
40	ACN9	ACN9 homolog (S. cerevisiae)	P376337	0,70 6,36E-04
41	RG9MTD1	RNA (guanine-9-) methyltransferase domain containing 1	P301994	0,70 1,88E-04
42				
43				
44				
45				
46				
47				
48				
49				
50				
51				
52				
53				
54				
55				
56				
57				
58				
59				
60				

Villeneuve et al.

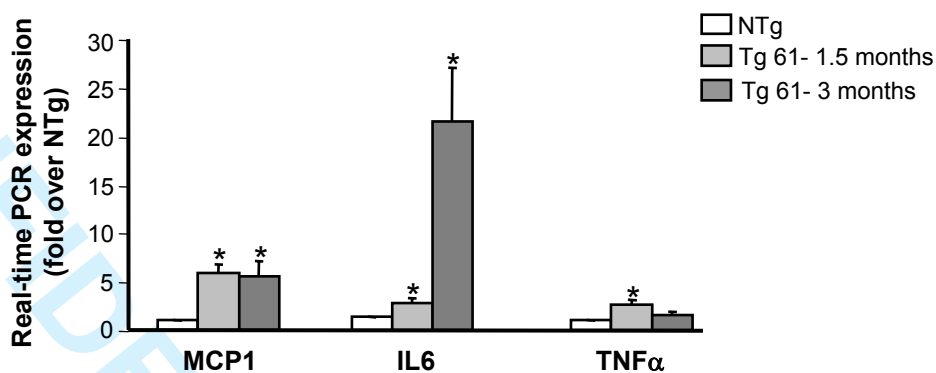
1					
2					
3	OXA1L	oxidase (cytochrome c) assembly 1-like	P531829	0,70	3,27E-04
4	MRPL49	mitochondrial ribosomal protein L49	P261351	0,70	4,52E-06
5	MTCP1	mature T-cell proliferation 1	P452280	0,70	6,41E-05
6		translocase of outer mitochondrial membrane 40			
7	TOMM40L	homolog (yeast)-like	P86003	0,70	2,06E-04
8	MRPL42	mitochondrial ribosomal protein L42	P40367	0,71	1,11E-03
9	GLRX2	glutaredoxin 2	P514107	0,71	8,98E-04
10					
11					
12					
13					
14					
15					
16					
17					
18					
19					
20					
21					
22					
23					
24					
25					
26					
27					
28					
29					
30					
31					
32					
33					
34					
35					
36					
37					
38					
39					
40					
41					
42					
43					
44					
45					
46					
47					
48					
49					
50					
51					
52					
53					
54					
55					
56					
57					
58					
59					
60					



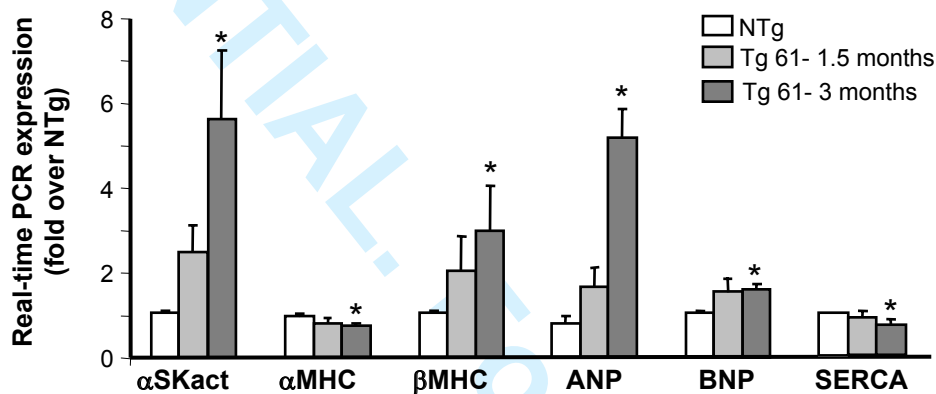
1
2
3
4
5
6
7
8
9
10
11
12
13
14
15
16
17
18
19
20
21
22
23
24
25
26
27
28
29
30
31
32
33
34
35
36
37
38
39
40
41
42
43
44
45
46
47
48
49



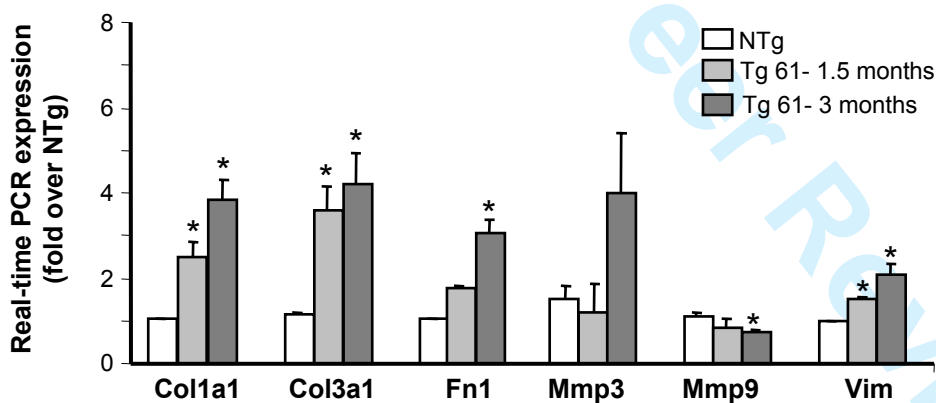
A



B



C



1
2
3
4
5
6
7
8
9
10
11
12
13
14
15
16
17
18
19
20
21
22
23
24
25
26
27
28
29
30
31
32
33
34
35
36
37
38
39
40
41
42
43
44
45
46
47
48
49
50
51
52
53
54
55
56
57
58
59
60

